the plant journal

SEB SOCIETY FOR EXPERIMENTAL BIOLOGY

The Plant Journal (2023) **114,** 591–612 doi: 10.1111/tpj.16155

Puncta-localized TRAF domain protein TC1b contributes to the autoimmunity of *snc1*

Kevin Ao[1,2], Philipp F. W. Rohmann[3,4], Shuai Huang[5], Lin Li[6], Volker Lipka[7,8], She Chen[6], Marcel Wiermer[3,4] and Xin Li[1,2,*]

[1]*Michael Smith Laboratories, University of British Columbia, Vancouver, British Columbia, V6T 1Z4, Canada,*
[2]*Department of Botany, University of British Columbia, Vancouver, British Columbia, V6T 1Z4, Canada,*
[3]*Molecular Biology of Plant-Microbe Interactions Research Group, Albrecht-von-Haller-Institute for Plant Sciences, University of Goettingen, D-37077, Goettingen, Germany,*
[4]*Biochemistry of Plant-Microbe Interactions, Dahlem Centre of Plant Sciences, Institute of Biology, Freie Universität Berlin, 14195, Berlin, Germany,*
[5]*Department of Molecular Genetics, College of Arts and Sciences, Ohio State University, Columbus, Ohio 43210, USA,*
[6]*National Institute of Biological Sciences, Beijing 102206, China,*
[7]*Department of Plant Cell Biology, Albrecht-von-Haller-Institute for Plant Sciences, University of Goettingen, D-37077, Goettingen, Germany, and*
[8]*Central Microscopy Facility of the Faculty of Biology and Psychology, University of Goettingen, D-37077, Goettingen, Germany*

Received 7 June 2022; accepted 7 February 2023; published online 17 February 2023.
*For correspondence (e-mail xinli@msl.ubc.ca).

SUMMARY

Immune receptors play important roles in the perception of pathogens and initiation of immune responses in both plants and animals. Intracellular nucleotide-binding domain leucine-rich repeat (NLR)-type receptors constitute a major class of receptors in vascular plants. In the *Arabidopsis thaliana* mutant *suppressor of npr1-1, constitutive 1* (*snc1*), a gain-of-function mutation in the NLR gene *SNC1* leads to SNC1 overaccumulation and constitutive activation of defense responses. From a CRISPR/Cas9-based reverse genetics screen in the *snc1* autoimmune background, we identified that mutations in *TRAF CANDIDATE 1b* (*TC1b*), a gene encoding a protein with four tumor necrosis factor receptor-associated factor (TRAF) domains, can suppress *snc1* phenotypes. TC1b does not appear to be a general immune regulator as it is not required for defense mediated by other tested immune receptors. TC1b also does not physically associate with SNC1, affect SNC1 accumulation, or affect signaling of the downstream helper NLRs represented by ACTIVATED DISEASE RESISTANCE PROTEIN 1-L2 (ADR1-L2), suggesting that TC1b impacts *snc1* autoimmunity in a unique way. TC1b can form oligomers and localizes to punctate structures of unknown function. The puncta localization of TC1b strictly requires its coiled-coil (CC) domain, whereas the functionality of TC1b requires the four TRAF domains in addition to the CC. Overall, we uncovered the TRAF domain protein TC1b as a novel positive contributor to plant immunity.

Keywords: plant immunity, autoimmunity, nucleotide-binding domain leucine-rich repeat (NLR) receptors, tumor necrosis factor receptor-associated factor (TRAF), meprin and TRAF-C homology (MATH), *suppressor of npr1-1, constitutive* (*snc1*), biomolecular condensates, CRISPR/Cas9, Arabidopsis thaliana, genetics.

INTRODUCTION

Microbial plant pathogens can deliver effector proteins into host cells to suppress plant immunity and promote virulence. Plant genomes encode a large collection of nucleotide-binding domain leucine-rich repeat-containing (NLR) receptors which can directly or indirectly recognize the presence or biochemical activity of pathogen effectors to activate downstream defensive responses (El Kasmi, 2021; Jones et al., 2016; Saur et al., 2021). Based on their differentiating N-terminal domain, major classes of NLRs include Toll/Interleukin-1 receptor (TIR)-type NLRs (TNLs), coiled-coil (CC)-type NLRs (CNLs), and RPW8-like CC-type helper NLRs (CC_R-hNLRs). TNLs signal through two parallel downstream pathways. One consists of the lipase-like proteins ENHANCED DISEASE SUSCEPTIBILITY 1 (EDS1) and PHYTOALEXIN DEFICIENT 4 (PAD4), which associates with the

ACTIVATED DISEASE RESISTANCE PROTEIN 1 (ADR1) family of CC_R-hNLRs (Dongus & Parker, 2021; Lapin et al., 2020; Wagner et al., 2013; Wu et al., 2021). TNLs such as SUPPRESSOR OF NPR1-1, CONSTITUTIVE 1 (SNC1), CHILLING-SENSITIVE MUTANT 1 (CHS1), and RECOGNITION OF PERONOSPORA PARASITICA 4 (RPP4) mainly rely on the EDS1/PAD4/ADR1s module (Aarts et al., 1998; Dong, Tong, et al., 2016; Glazebrook et al., 1997; Li et al., 2001; van der Biezen et al., 2002; Wang et al., 2013; Wu et al., 2019; Zhang et al., 2003). The second pathway consists of the lipase-like proteins EDS1 and SENESCENCE-ASSOCIATED GENE 101 (SAG101), which associates with the N REQUIREMENT GENE 1 (NRG1) family of CC_R-hNLRs (Feys et al., 2005; Lapin et al., 2019; Sun et al., 2021; Wagner et al., 2013). CHS3 is an example of a TNL that relies mostly on the EDS1/SAG101/NRG1s module (Wu et al., 2019; Xu et al., 2015).

Current working models suggest that effector recognition by TNLs results in a conformational change which promotes TNL oligomerization into higher-order complexes called resistosomes and induces proximity of the TNL TIR domains (Duxbury et al., 2020; Ma et al., 2020; Martin et al., 2020; Williams et al., 2014; Zhang et al., 2017). Interestingly, TIR domains have been shown to exhibit enzymatic activities yielding various small molecules that are recognized by downstream components EDS1/PAD4/SAG101, which subsequently activate CC_R-hNLRs ADR1s and NRG1s (Horsefield et al., 2019; Huang et al., 2022; Jia et al., 2022; Lapin et al., 2022; Manik et al., 2022; Wan et al., 2019; Yu et al., 2022). It is thought that activation of CC_R-hNLRs leads to the formation of a multimeric wheel-like resistosome with membrane channel function, which triggers downstream signaling events (Jacob et al., 2021). Interestingly, some NLRs also associate with transcriptional co-repressors and transcription factors that are required for NLR function, suggesting that NLRs may also directly activate transcriptional changes inside nuclei (Cui et al., 2015; Sun et al., 2020; Tsuda & Somssich, 2015).

One well-studied TNL is SNC1 from *Arabidopsis thaliana* (hereafter Arabidopsis). The *snc1* mutant contains a gain-of-function (g-o-f) mutation which stabilizes SNC1 protein, resulting in the constitutive activation of defense responses and autoimmunity-related dwarfism (Cheng et al., 2011; Zhang et al., 2003). Various forward and reverse genetic screens using *snc1* and other backgrounds revealed the importance of pre/post-transcriptional/translational control, nucleocytoplasmic transportation, and protein homeostasis in NLR regulation (Johnson et al., 2012; Li et al., 2015). For example, two close homologs, MUTANT, SNC1-ENHANCING 13 (MUSE13) and MUSE14, were identified from a *snc1* forward genetic screen and shown to facilitate SNC1 protein turnover via the 26S proteasome likely by interacting with proteins required for SNC1 degradation (Huang et al., 2016).

Although remarkable progress has been made in understanding NLRs and TNLs in general, our understanding of SNC1 regulation and downstream signaling is still incomplete. One possible reason for why only a limited number of signaling genes were found through forward genetic screens in *snc1* is genetic redundancy, which impedes gene discovery in mutagenesis-based screens. An alternative genetics strategy that circumvents this problem is to use targeted reverse genetic screens to investigate the function of candidate immune-related families.

The tumor necrosis factor receptor (TNF-R)-associated factor (TRAF) domain, also referred to as the meprin and TRAF-C homology (MATH) domain, is a protein–protein interaction structure that can be found in diverse species (Zapata et al., 2007). TRAF regions are present in multiple members of a mammalian E3 ubiquitin ligase family, including TRAF1 to TRAF6, which serve as key signaling components downstream of many receptors including NLRs, Toll-like receptors (TLRs), retinoic acid-inducible gene-I (RIG-I)-like receptors (RLRs), T-cell receptors, and various cytokine receptors (e.g., the interleukin-1 receptor family and TNF-R) (Park, 2018; Xie, 2013). These proteins serve both as a scaffold to link receptors with downstream signaling components (kinases, ubiquitin ligases) and as an E3 ligase that mediates K63-linkage polyubiquitination of various substrates (Park, 2018; Xie, 2013).

Interestingly, compared with mammals, plants possess a vastly expanded TRAF domain-containing protein family, though most lack the E3 ligase domain found in many human TRAFs. The Arabidopsis genome encodes more than 100 TRAF proteins, many of which are tandemly encoded in the genome or have close homologs (Kushwaha et al., 2016; Oelmüller et al., 2005; Qi et al., 2022; Zhao et al., 2013). Such a genomic pattern is reminiscent of the genomic organization of NLR gene clusters in higher plants, which can contain a few to tens of NLR genes (Barragan & Weigel, 2021). The involvement of some TRAF family members in plant development, abiotic stress, and plant immunity has been previously reported (Kushwaha et al., 2016; Qi et al., 2022). In particular, MUSE13/14 are TRAF proteins that contribute to plant immunity (Huang et al., 2016). However, the functions of most plant TRAF proteins have not been explored. Given the parallels between mammalian and plant immunity, and since mammalian TRAF proteins work as immune adapters and signal transducers downstream of NLRs and TIR domain-containing TLRs (Park, 2018; Xie, 2013), we hypothesized that additional plant TRAF proteins may play a role in the regulation or signaling of TIR-containing TNLs like SNC1.

With the development of CRISPR/Cas9 as an efficient genome-editing tool in plants, we took advantage of this technology to study the potential involvement of the TRAF gene family in plant immunity in more detail. We carried

out a reverse genetic screen where we created multi-gene knockout mutations of members of the TRAF gene family in *snc1*, in order to find suppressor or enhancer candidates directly involved in innate immunity. Here we describe one gene recovered from this screen, *TRAF CANDIDATE 1b* (*TC1b*), which is required for full *snc1* autoimmunity. TC1b is not required for the phenotypes of other tested autoimmune mutants, for the protein homeostasis of SNC1, or for ADR1-mediated downstream signaling. Thus, TC1b is a novel component of plant immunity involved in the regulation or activation of SNC1.

RESULTS

A reverse genetic screen to identify regulators of immunity

We first generated and analyzed a list of TRAF domain proteins from 19 representative species, including both plants and animals, using the UniProt and InterPro databases (Jones et al., 2014; Mitchell et al., 2019; UniProt Consortium, 2019) (Table S1). A domain phylogeny was inferred using the peptide sequences of the TRAF domains from these proteins (Figure S1). We grouped the proteins into 11 subfamilies taking into account previous classifications (Kushwaha et al., 2016; Qi et al., 2022; Zapata et al., 2007; Zhao et al., 2013), PANTHERdb classifications (Thomas et al., 2022), and our own phylogenetic analysis (Figures S1 and S2, Table S1). In order to shortlist candidate genes, we leveraged publicly available microarray data to identify TRAF genes that are induced or repressed upon pathogen or elicitor treatment, or that are regulated by master immune-related transcription factors like SARD1 (Sun et al., 2015; Waese et al., 2017). There were no clades that obviously stood out when considering induction/repression patterns upon different biotic treatment, potentially because many of the genes were not represented in the microarrays (Table S2). Because this may potentially cause us to miss interesting candidates, we also took a more general approach and considered other factors like gene clustering and interesting domain architectures when selecting genes (Figures S2 and S3). Through these analyses, we chose 13 candidate clades/groups with hypothesized immune function for further analysis (Figure S3, Table S3). CRISPR constructs were designed to delete these genes either individually (unlinked genes) or as a cluster (tandemly encoded genes). CRISPR deletion constructs were transformed into the sensitized autoimmune *snc1* background to enable the recovery of both positive and negative regulators of immunity (Figure S4).

Mutations in *TC1b* suppress *snc1*

Here, we report on one candidate isolated from the screen. A CRISPR construct containing one sgRNA was designed to mutate a pair of neighboring genes encoding TRAF domain proteins, *AT2G25330* and *AT2G25320*, which we hereafter refer to as *TRAF CANDIDATE 1a* (*TC1a*) and *TC1b*, respectively (Figure 1a). The sgRNA (sgRNA1) targets an identical sequence region in the first exon of *TC1a* and *TC1b* (Figure 1a, Tables S4 and S5). The sgRNA does not identically match anywhere else in the genome, ensuring target specificity (Table S5). The *TC1a/b* CRISPR construct was transformed into *snc1* plants, and 10 T1 lines were individually followed. The T2 progeny from two independent T1 lines segregated for a partial *snc1* suppression phenotype. Deletion PCR was carried out on the dwarfism-suppressing plants using primers flanking the predicted deletion region (Table S4). Deletion bands could only be detected in plants originating from one T1 line, suggesting that the other may contain point mutations. T2 plants from different T1 lines exhibiting the suppression phenotype were followed to the T3 generation, and the lines were screened for homozygosity of the suppression phenotype and absence of the CRISPR cassette using PCR. Single T3 plants were kept for further analysis and named *tc1ab-1 snc1* and *tc1ab-2 snc1* (Figure 1b).

To determine whether the isolated lines also exhibited suppressed disease resistance compared to *snc1*, we challenged the plants with the biotrophic oomycete pathogen *Hyaloperonospora arabidopsidis* (*H.a.*) Noco2. The suppressor lines were more susceptible to *H.a.* Noco2 compared with *snc1* (Figure 1c). Through Sanger sequencing (Table S4), we found that the first line, *tc1ab-1 snc1*, contains a 3585-bp deletion between *TC1a* and *TC1b*, whereas the second line, *tc1ab-2 snc1*, carries a 1-bp deletion each in *TC1a* and *TC1b* (Figure 1d). The mutations in both lines cause frameshifts and premature stop codons (Figure S5).

To test whether mutations in both genes are required for the *snc1* suppression phenotype, mutants containing T-DNA insertions in the exons of these genes were obtained (Figure 1a). When SALK_103885c (renamed *tc1a-1*), which carries a T-DNA insertion in the first exon of *TC1a*, was crossed with *snc1*, the double mutant plants resembled *snc1* in morphology and weight (Figure 1e,f). However, when *CS356847* (renamed *tc1b-1*), which carries a T-DNA insertion in the fourth exon of *TC1b*, was crossed with *snc1*, the double mutant plants were larger than *snc1* and resembled *tc1ab-1 snc1* plants (Figure 1e,f). Furthermore, the suppression phenotype co-segregated with homozygosity of the *tc1b-1* T-DNA allele. Thus, loss of *TC1b* but not *TC1a* can suppress *snc1*.

As portions of *TC1a*/*TC1b* could still be expressed in the *tc1ab-1*, *tc1ab-2*, and *tc1b-1* alleles, we considered whether the partial *snc1* suppression phenotypes in the presence of these alleles are due to incomplete disruption of the genes. A second round of CRISPR mutagenesis, using an egg cell promoter-driven Cas9 construct (Wang et al., 2015; Xing et al., 2014) and sgRNA2/3, was performed to fully delete both genes (Figure 1a, Table S5). Deletion-

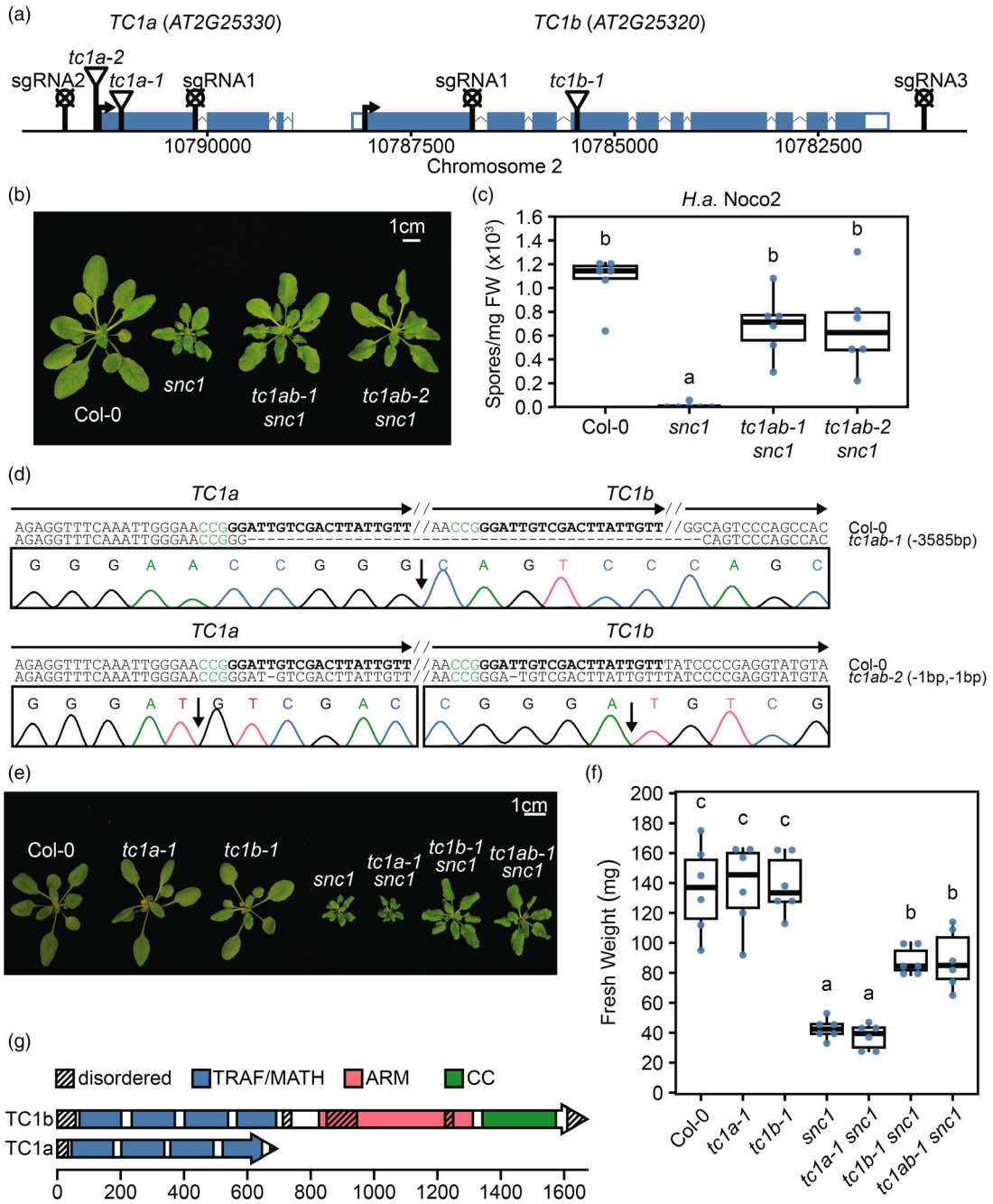

Figure 1. TC1b, a TRAF-ARM-CC protein, is required for full *snc1* autoimmunity.
(a) Gene diagram depicting gene models of *TC1a* and *TC1b* in their relative genomic context. Exons (filled blue rectangles), untranslated regions (empty rectangles), and introns (chevrons) are represented. Notable sites, such as T-DNA insertion sites (triangles) and CRISPR sgRNA target sites (circles with X), are highlighted. Numbers on the axis represent chromosomal coordinates. Arrows represent direction of translation.
(b) Morphology of 3.5-week-old soil-grown plants: WT (Col-0), *snc1*, and two independent CRISPR gene-edited plants in the *snc1* background. Scale bar is 1 cm.
(c) Quantification of *H.a.* Noco2 sporulation on the indicated genotypes 7 days post-inoculation with 10^5 spores mL^{-1}.
(d) *TC1a*/*b* mutations in *tc1ab-1 snc1* and *tc1ab-2 snc1* plants. Gene direction (horizontal arrow), PAM sequences (green text), sgRNA target sites (bold text), mutation sites (vertical arrow), sequences hidden for conciseness (//), and deleted bases (–) are marked. Deletion sizes of alleles are indicated in parentheses on the right. Sanger sequencing chromatograms are provided below the mutant allele sequence.
(e) Morphology of 3-week-old soil-grown plants of the indicated genotypes. Scale bar is 1 cm.
(f) Quantification of fresh weight of plants from (e).
(g) A protein diagram of TC1a and TC1b (white arrow in N-to-C orientation) and their predicted domains (colored) drawn to scale. Numbers on the axis represent protein/domain length in amino acids.
Box plots in (c) and (f) are overlaid with dot plots of original data points ($n = 6$). Means not sharing any letter are significantly different ($P < 0.05$), determined using one-way ANOVA with the post-hoc Tukey HSD test.

flanking primers were used to screen T1 plants for deletions by PCR. Homozygous deletion and transgene-free plants were identified in the T2 generation and kept for further analysis. *snc1* plants with the full *TC1a*/*TC1b* locus deleted (*tc1ab-3 snc1* to *tc1ab-6 snc1*) still resembled *tc1b-1 snc1* in morphology and weight, confirming that only *TC1b* is required for *snc1* autoimmunity (Figure S6a,b).

TC1b is an ancient gene and can be found in early diverging species including some green algae (Figure S7a). On the other hand, *TC1a* is a recent duplication of *TC1b*, and is only present in a relatively small clade of Brassicaceae species (Figure S7a,b). *TC1a* is absent in the *Brassica* genus but is present in some close Arabidopsis relatives (Figure S7b). Moreover, at least 70 ecotypes of Arabidopsis contain alleles of *TC1a* that have high-impact single-nucleotide polymorphisms (SNPs) and insertions/deletions (indels), compared to one ecotype carrying a deleterious *TC1b* allele, further suggesting that TC1a function is dispensable (Figure S7c).

TC1b encodes a protein with four tandemly repeated TRAF domains, a central ARMADILLO (ARM)-type fold, and a long C-terminal CC domain (Figure 1g). The protein also possesses numerous predicted disordered regions. *TC1a* shares a similar gene architecture with the 5′ end of *TC1b* but is truncated (Figure 1a). As a result, TC1a only possesses the four TRAF domains (Figure 1g). The N-terminal TRAF domains of TC1a and TC1b are highly similar, sharing 81% identity and 87% similarity (and 35% identity and 38% similarity overall). TC1a and TC1b are the sole members of this subfamily of TRAF domain-containing proteins in Arabidopsis (Zapata et al., 2007; Zhao et al., 2013).

Overexpression of TC1b can enhance *snc1* phenotypes and cause autoimmunity in wild-type plants

Since loss of *TC1b* can suppress *snc1* phenotypes, we examined whether overaccumulation of *TC1b* can lead to the opposite effect. Indeed, *snc1* plants overexpressing *p35S::TC1b-FLAG* exhibited enhanced dwarfism compared with *snc1* (Figure 2a,b). Consistently, the enhanced dwarfism phenotype co-segregated with the presence of the transgene. TC1b-FLAG protein of the predicted size could be detected in the overexpression plants, suggesting that the phenotype is due to overaccumulation of the full-length protein (Figure 2c). In addition, stable transgenic lines overexpressing *p35S::TC1b-FLAG* in the wild-type (WT) background were stunted in stature (Figure 2b,d) and exhibited enhanced resistance to *H.a.* Noco2 (Figure 2e). These phenotypes are most likely caused by the overexpression of full-length TC1b-FLAG protein (Figure 2f). Thus, TC1b is a positive regulator of plant immunity.

TC1b does not play a general role in receptor-mediated immunity or basal immunity

Many previously characterized suppressors/enhancers of *snc1* and other autoimmune mutants are general immune regulators (Johnson et al., 2012; Li et al., 2015). Others play specific roles in NLR-mediated defense pathways (Cheng et al., 2011; Gou et al., 2012). To determine which category of regulator TC1b belongs to, autoimmune mutants activating different pathways were used for epistasis analysis (van Wersch et al., 2016). Cell surface pattern recognition receptors (PRRs), including receptor-like proteins (RLPs), are receptors that mediate perception of extracellular signals (Albert et al., 2020). *snc2-1D* is a g-o-f mutant of the RLP SNC2 that causes constitutive activation of SNC2 defense pathways and autoimmunity (Zhang et al., 2010). *tc1b-1* could not suppress *snc2-1D phenotypes*, suggesting that *TC1b* is not involved in the pathways of RLPs like SNC2 (Figure 3a). MEKK1 is a component of a MAP kinase cascade that is guarded by the CNL SUMM2. In *mekk1-5*, disruption of MEKK1 results in constitutive activation of SUMM2 and autoimmunity (Bjornson et al., 2014; Zhang et al., 2012). *tc1b-1* could not suppress the stunted stature of *mekk1-5*, suggesting that *TC1b* may not work downstream of CNLs like SUMM2 (Figure 3b). *chs3-2D* is a g-o-f mutant of the atypical TNL CHS3, which mainly relies on the EDS1/SAG101/NRG1s downstream module (Bi et al., 2011; Wu et al., 2019). *tc1b-1* could not suppress the severe dwarfism of *chs3-2D*, suggesting that *TC1b* may not be required for NRG1s-dependent TNLs (Figure 3c). Similar to *snc1*, the typical TNL RPP4 and the truncated TNL (TN) protein CHS1 both mainly rely on the EDS1/PAD4/ADR1s module (Wu et al., 2019). *chs2-1*, a dominant mutant of RPP4, and *chs1-2*, a g-o-f mutant of CHS1, both exhibit autoimmunity-related dwarfism and cell death when grown at low temperatures (Huang et al., 2010; Wang et al., 2013). *tc1b-1* could not suppress the cold-induced cell death of c*hs2-1* or *chs1-2* (Figure 3d,e), suggesting that *TC1b* may not be required for other ADR1-dependent TNLs besides SNC1. Thus, *TC1b* does not seem to be generally required for receptor-mediated defense.

To investigate whether *TC1b* may play a role in basal immunity against pathogens, we challenged *tc1ab-1* plants with the virulent bacterial pathogen *Pseudomonas syringae* pv. *tomato* (*P.s.t.*) DC3000. *tc1ab-1* plants were not more susceptible to this pathogen compared with WT, as opposed to *eds1-2* plants (Figure 3f). We also further examined whether *TC1b* is required for cell surface receptor-mediated immunity. The *P.s.t.* DC3000 *hrcC*$^{-}$ strain is deficient in effector delivery due to the loss of a type III secretion system component (Yuan & He, 1996). This strain has been used to investigate PRR immunity independent of effector presence. As compared to *agb1-2*, which contains a T-DNA insertion in a G-protein β-subunit gene necessary for the signaling of PRRs (Liu et al., 2013; Ullah et al., 2003), *tc1b-1* plants were not more susceptible to *P.s.t.* DC3000 *hrcC*$^{-}$. Upon recognition of their ligand, PRRs activate a series of downstream responses leading to immunity-promoting transcriptional changes. For example,

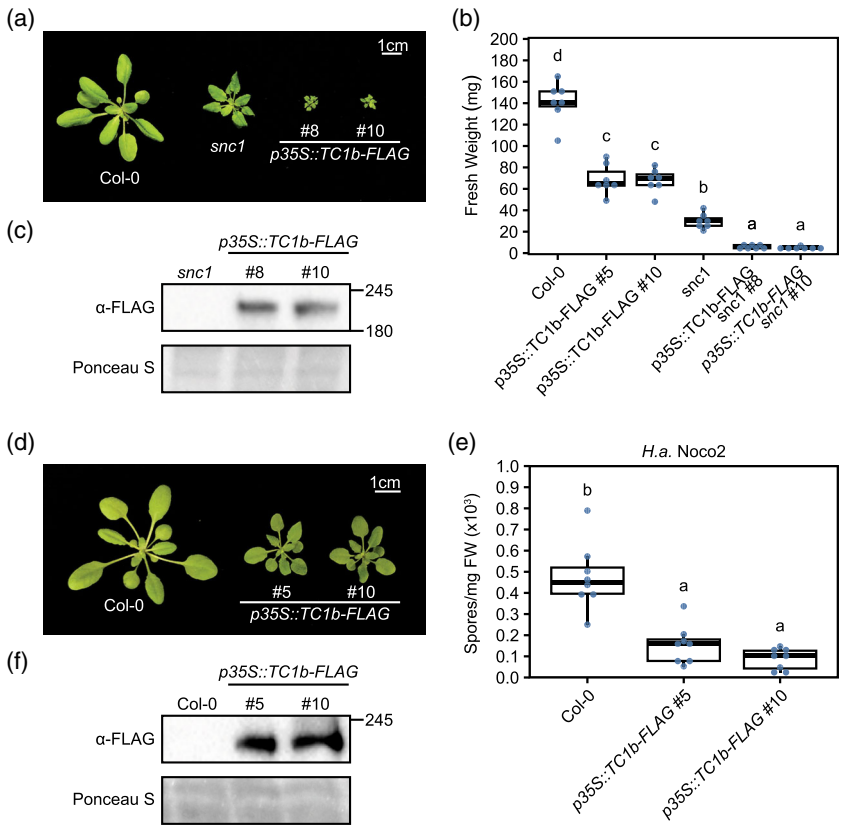

Figure 2. Overexpression of TC1b results in autoimmunity and enhances *snc1* dwarfism.
(a, d) Morphology of 3.5-week-old soil-grown plants of indicated genotypes. Scale bar is 1 cm.
(b) Quantification of fresh weight of genotypes from (a) and (d) ($n = 7$).
(c, f) Western blot analysis of TC1b-FLAG protein levels in genotypes shown in (a) and (d), respectively. Ponceau S staining serves as a loading control. Protein sizes in kDa are indicated to the right.
(e) Quantification of *H.a.* Noco2 sporulation on the indicated genotypes 7 days post-inoculation with 2×10^4 spores mL^{-1} ($n = 8$). Box plots are overlaid with dot plots of raw data points. Means not sharing any letter are significantly different ($P < 0.05$), determined using one-way ANOVA with the post-hoc Tukey HSD test.

treatment with the flagellin epitope flg22, which is recognized by the PRR FLS2, leads to the expression of *FMO1*, a key gene required for biosynthesis of the plant defense hormone *N*-hydroxypipecolic acid (Gómez-Gómez & Boller, 2000; Hartmann et al., 2018; Tian et al., 2021). Transcriptional activation of *FMO1* was unaffected in the *tc1b-1* and *tc1ab-1* mutants 4 h after flg22 treatment, but was abolished in the *FLS2* mutant *fls2c efr-1 cerk1-2* (Figure 3h). Overall, TC1b does not seem to be a general immune regulator, since it is not required for TNL, CNL, and PRR pathways and is not required for basal resistance.

TC1b acts upstream of *ADR1*s and *EDS1*

Since TC1b is not required for other immune receptor-mediated pathways, we focused on how TC1b affects SNC1-related autoimmunity. First, we investigated whether loss of TC1b affects SNC1 downstream signaling. SNC1 mainly signals through the EDS1/PAD4/ADR1s module (Wu et al., 2019; Zhang et al., 2003). An Asp-to-Val mutation in the MHD motif of the helper NLR ADR1-L2 results in autoactivation of the ADR1-L2 pathway and autoimmunity (Roberts et al., 2013). We tested whether TC1b is required for the autoimmunity of *ADR1-L2*^{D484V}-expressing plants. *tc1b-1 ADR1-L2*^{D484V} plants are similar in stature to *ADR1-L2*^{D484V} plants (Figure 4a), suggesting that TC1b does not act downstream of the ADR1s.

Because TC1b-FLAG overexpression lines are autoimmune, we took advantage of this phenotype to determine if *EDS1* is required for *TC1b*-dependent autoimmunity and whether TC1b acts upstream of EDS1 signaling. Loss of *EDS1* has been previously shown to completely suppress the *snc1* autoimmune phenotypes due to the requirement of EDS1 for SNC1 downstream signaling through helper NLRs (Dong, Tong, et al., 2016; Li et al., 2001; Wu et al., 2019). *eds1-25* is a newly generated loss-of-function allele of *EDS1a/b* carrying a deletion of both *EDS1a* and *EDS1b* (Figure S8) generated by CRISPR/Cas9 using a previously described construct (Tian et al., 2021). *snc1 eds1-25* lines are WT-like, confirming that *EDS1* has been deleted (Figure 4b). The short stature of *p35S::TC1b-FLAG* #10 lines is suppressed in *p35S::TC1b-FLAG* #10 *snc1 eds1-25* lines,

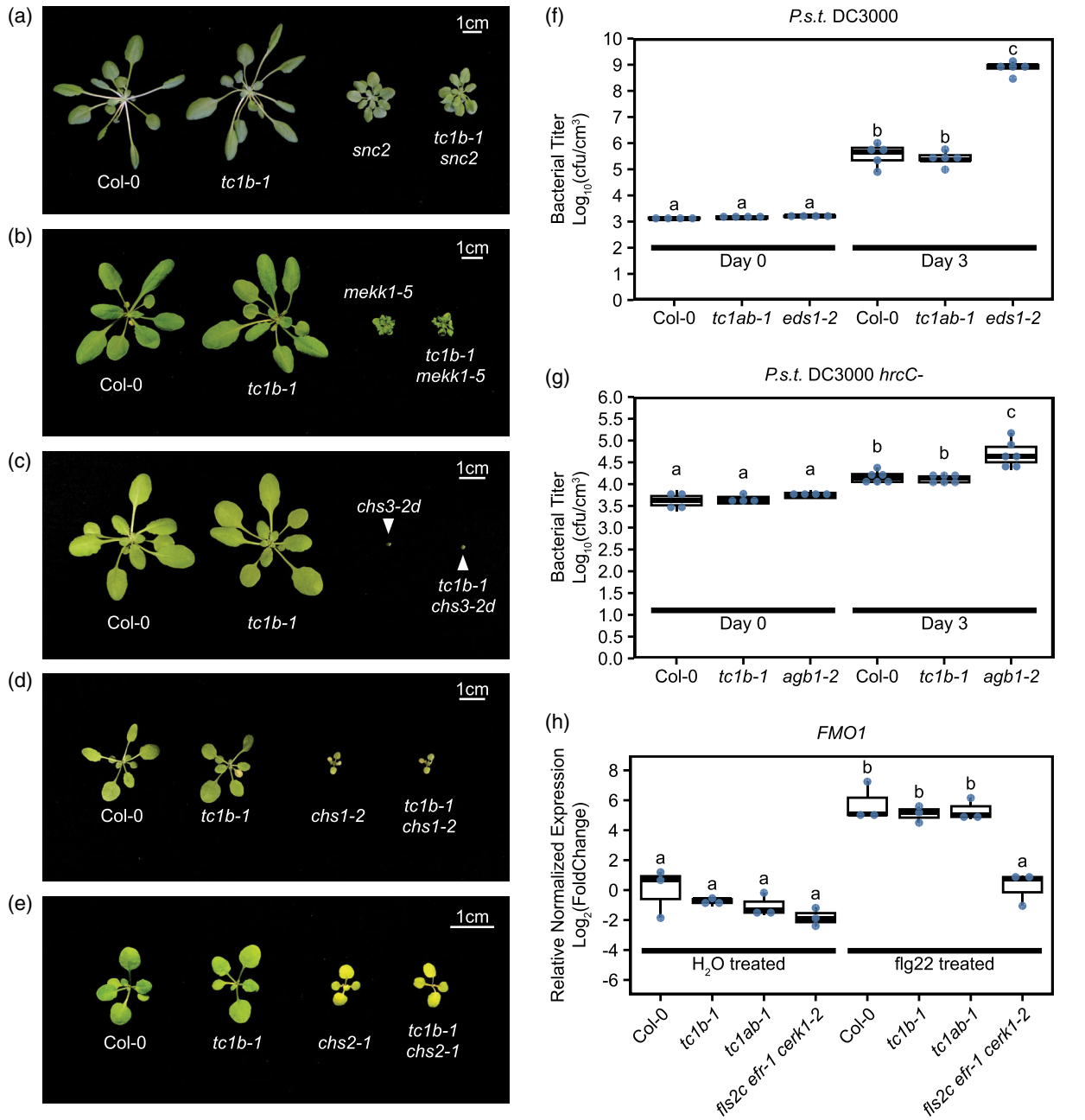

Figure 3. TC1b does not contribute to the signaling pathways of tested immune receptors.
(a–c) Morphology of 3.5-week-old soil-grown plants of the indicated genotypes. Scale bar is 1 cm.
(d) Morphology of 2.5-week-old soil-grown plants of the indicated genotypes. Plants were grown at 22°C under long-day conditions for 10 days and then at 16°C under short-day conditions for 7 days. Scale bar is 1 cm.
(e) Morphology of 2.5-week-old soil-grown plants of the indicated genotypes. Plants were grown at 22°C under long-day conditions for 10 days and then at 10°C under continuous light for 7 days. Scale bar is 1 cm.
(f, g) Quantification of *Pseudomonas syringae* pv. *tomato* (*P.s.t.*) DC3000 and *P.s.t.* DC3000 *hrcC*⁻ growth in leaves of 4-week-old plants of the indicated genotypes. Plants were infiltrated with a bacterial inoculum of OD_{600} = 0.0001 and 0.002, respectively. Bacterial titer was measured at 0 and 3 days post-infiltration.
(h) Expression of *FMO1* 4 h after mock (H_2O) or 1 μM flg22 treatment of indicated plants. Values represent expression relative to *ACT7*, normalized to WT mock-treated plants.
Box plots in (f), (g), and (h) are shown with dot plots of values overlaid. Means not sharing any letter are significantly different ($P < 0.01$), determined using one-way ANOVA with the post-hoc Tukey HSD test.

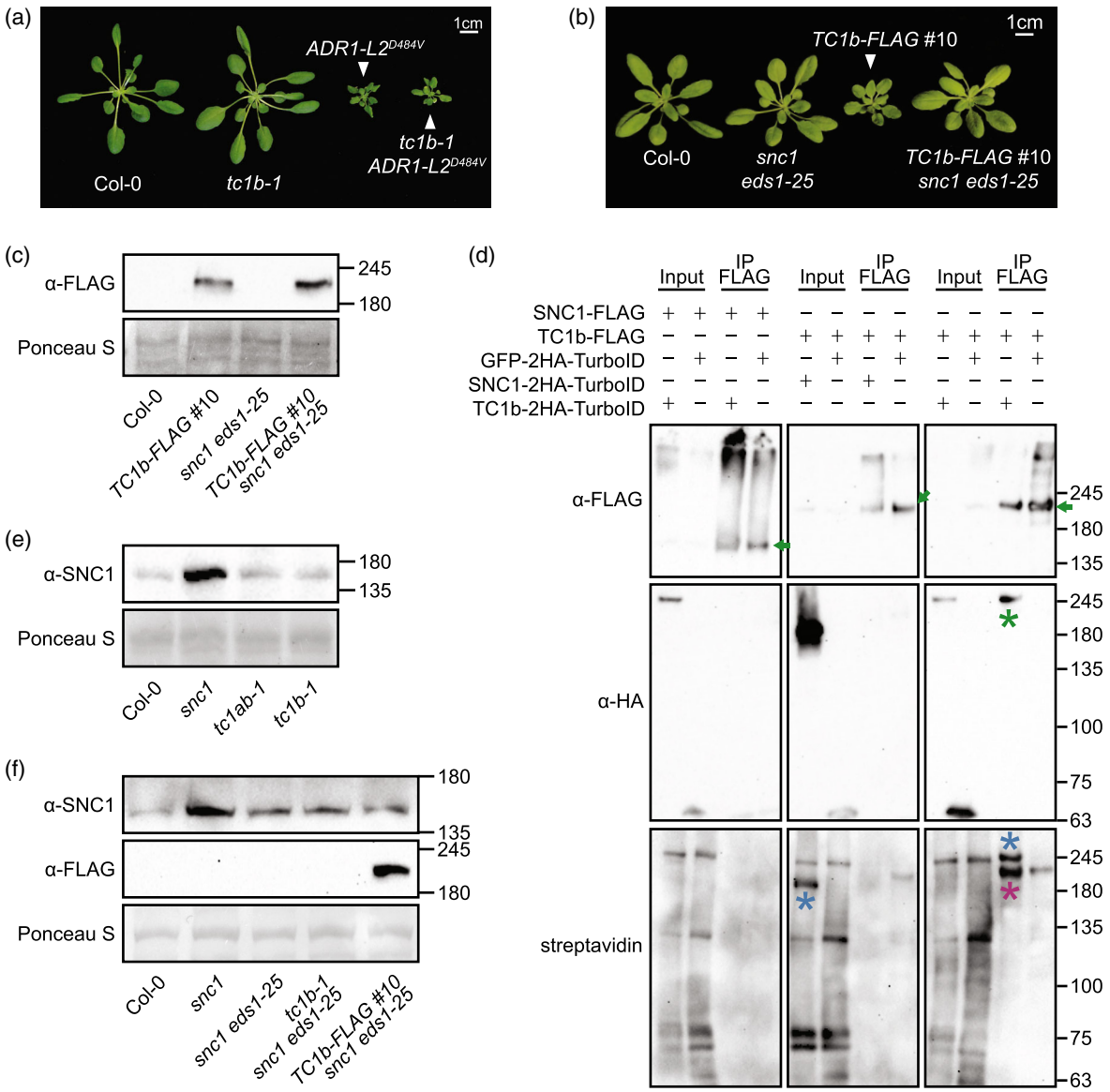

Figure 4. TC1b acts upstream of ADR1s/EDS1, but does not interact with SNC1 or affect SNC1 protein levels.
(a, b) Morphology of 3.5-week-old soil-grown plants of the indicated genotypes. Scale bar is 1 cm.
(c, e, f) Western blot analysis of TC1b-FLAG (c and f) or SNC1 (e and f) protein levels in indicated lines. Reference molecular mass markers are shown on the right in kDa. Ponceau S staining serves as a loading control.
(d) TurboID proximity labeling assay of *Nicotiana benthamiana*-expressed SNC1-FLAG or TC1b-FLAG with GFP-2HA-TurboID, TC1b-2HA-TurboID, or SNC1-2HA-TurboID. FLAG-tagged proteins were immunoprecipitated using anti-FLAG beads. Proteins were detected using indicated antibodies or streptavidin-HRP. Reference molecular mass markers are shown on the right in kDa. Input, total protein extract; IP FLAG, immunoprecipitated samples. Green arrows, immunoprecipitated FLAG-tagged protein; green asterisk, co-immunoprecipitated TurboID-tagged protein; blue asterisk, self-biotinylated TurboID-tagged protein; magenta asterisk, trans-biotinylated FLAG-tagged protein.

which morphologically resemble *snc1 eds1-25* and WT plants (Figure 4b). The suppression is not due to transgene silencing since TC1b-FLAG protein can still be detected (Figure 4c). Thus, activation of immunity by TC1b relies on EDS1.

TC1b does not interact with SNC1

Several regulators of SNC1 can directly interact with SNC1 (Cheng et al., 2011; Gou et al., 2012; Xu et al., 2014; Zhu et al., 2010). To test whether TC1b can associate with SNC1, a TurboID-based proximity labeling assay was used (Zhang et al., 2019). TurboID is a biotin ligase that can biotinylate proximal proteins in the presence of biotin (Branon et al., 2018). *tc1ab-1 snc1* plants overexpressing *p35S::TC1b-2HA-TurboID* exhibit enhanced dwarfism compared to *tc1ab-1 snc1*, suggesting that the fusion protein is functional (Figure S9a,b). TC1b-2HA-TurboID could not biotinylate or be co-immunoprecipitated (co-IPed) by SNC1-FLAG

(Figure 4d). In a reciprocal assay, SNC1-2HA-TurboID could not biotinylate or be co-IPed by TC1b-FLAG, but could self-biotinylate (Figure 4d). In contrast, TC1b-2HA-TurboID could biotinylate and be co-IPed by TC1b-FLAG, and could self-biotinylate (Figure 4d). These results suggest that TC1b does not associate with SNC1 but can form homo-oligomers. This is consistent with other TRAF proteins from plants and mammals that also exhibit self-oligomerization activity.

TC1b does not affect SNC1 protein levels

Multiple previous studies have revealed processes that modulate SNC1 function, including protein turnover, nucleocytoplasmic trafficking, and expression regulation (Johnson et al., 2012; Li et al., 2015). Many genes required for *snc1* autoimmunity affect protein homeostasis either directly (SNC1 degradation) or indirectly (reduced transcription). Since defects in SNC1 protein turnover or *SNC1* gene expression both affect SNC1 protein accumulation, we measured SNC1 levels in the *tc1b-1* and *tc1ab-1* lines. SNC1 protein levels were similar in *tc1b-1* plants compared with WT (Figure 4e). Since the level of SNC1 protein is quite low in WT plants and small differences may not be obvious, we also measured the SNC1 protein level in the *snc1 eds1-25* background. In *snc1 eds1-25*, SNC1 protein accumulation is higher but the confounding autoimmune positive feedback upregulation of *SNC1* is blocked by *eds1-25*. Through crossing, we generated lines where TC1b was knocked out (*tc1b-1 snc1 eds1-25*) or overexpressed (*p35S::TC1b-FLAG* #10 *snc1 eds1-25*) in order to examine the contribution of TC1b to SNC1 protein homeostasis. SNC1 protein levels were similar in *tc1b-1 snc1 eds1-25* and *p35S::TC1b-FLAG* #10 *snc1 eds1-25* plants compared to *snc1 eds1-25* (Figure 4f), suggesting that TC1b may not be involved in modulating SNC1 protein homeostasis or *SNC1* expression. However, we cannot completely rule out the possibility that TC1b contributes slightly to SNC1 homeostasis, as small differences cannot be detected by the approaches we used.

TC1b localizes to punctate structures

Multiple components necessary for *snc1* autoimmunity, including nuclear transport receptors and nuclear pore complex components, can affect the nucleocytoplasmic distribution of SNC1 (Cheng et al., 2009; Palma et al., 2005). Some have been shown to localize to the nuclear envelope or have nucleocytoplasmic distributions. To test whether TC1b is a nuclear or cytoplasmic regulator or whether TC1b is associated with the nuclear envelope, we investigated the subcellular localization of TC1b. *snc1* plants expressing either *p35S*- or *pTC1b*-driven fluorescent protein-tagged TC1b exhibited enhanced dwarfism, suggesting that the fusion proteins are functional and localize to the proper compartments (Figure S10a–d). Interestingly, despite the difference in promoters, plants expressing pTC1b::TC1b-2HA-GFP were as capable of activating immunity as *p35S* lines. Potentially, a negative regulatory element up/downstream of the gene may be missing in the native promoter construct. Alternatively, plants may be highly sensitive to small changes in TC1b protein levels, and the *pTC1b::TC1b-2HA-GFP* construct may exceed a minimum threshold. Because we could not consistently observe fluorescence in these Arabidopsis lines, we used a heterologous system. When transiently expressed in *Nicotiana benthamiana*, TC1b-YFP localizes in punctate structures in the cytoplasm of epidermal cells (Figure S10e). To ensure the localization was not a result of protein aggregation due to overexpression, a native promoter-driven pTC1b::TC1b-2HA-GFP construct was also used. TC1b-2HA-GFP was localized to similar puncta in *N. benthamiana* (Figure S10f), suggesting that these puncta are biologically relevant.

The observed puncta do not resemble ER or mitochondrial localization patterns. To identify whether these puncta correspond to other known subcellular compartments, we used fluorescently tagged markers for colocalization analysis. TC1b-YFP does not colocalize with the peroxisomal marker px-rb (Nelson et al., 2007), suggesting that these puncta are not peroxisomes (Figure S11a). Next, we wondered whether the puncta were related to endosomes and multi-vesicular bodies. Three markers were used to test this: mCherry-RabF2a, a late endosome/multi-vesicular body marker, mCherry-RabA1g, an endosome/recycling endosome marker, and mCherry-RabG3c, a late endosome marker (Geldner et al., 2009). None of the markers share a similar localization pattern with TC1b, and TC1b puncta do not coincide with the puncta observed with these markers (Figure S11b–d). Autophagosomes, which can be monitored using ATG proteins like ATG8e, also have a puncta localization pattern (Yoshimoto et al., 2004). Although puncta were observed with the autophagosome marker mCherry-ATG8e, they do not overlap with TC1b-YFP puncta. Finally, we considered stress granules, membraneless biomolecular condensates consisting of aggregates of proteins and RNA that can be induced upon cell stress (Maruri-López et al., 2021). The stress granule marker mCherry-RBP47B also does not share a localization pattern with TC1b-YFP, but a few mCherry-RBP47B puncta overlapped with TC1b-YFP puncta. It is unclear whether this overlap may be due to spectral cross-talk or bleed-through from particularly bright TC1b-YFP puncta or whether this reflects authentic colocalization. Overall, TC1b-YFP puncta largely do not appear to be peroxisomes, endosomal components, autophagosomes, or stress granules.

The CC domain is required for the punctate localization of TC1b

We also considered the possibility that TC1b may localize to a unique compartment. TC1b possesses multiple

domains, TRAF, ARM, and CC, which have all been shown to be involved in homotypic and/or heterotypic protein–protein interactions in other proteins. It is possible that the puncta are large hetero- or homo-oligomeric complexes. A second hypothesis is based on the observation that the properties of these puncta are reminiscent of membraneless organelles (liquid–liquid phase separated compartments). Proteins that undergo liquid–liquid phase transitions usually possess domains like intrinsically disordered regions and CC domains that drive the formation of these structures (Fang et al., 2019; Lu et al., 2020; Uversky, 2017). TC1b was predicted to contain disordered regions and a CC domain (Figure 1g). To test the requirement of these regions for TC1b subcellular localization, we generated TC1b-YFP domain truncations (Figure 5a). Deletion of the N-terminal disordered region or the ARM domain did not abolish the localization of TC1b-YFP (Figure 5a,b). Although increased cytoplasmic signal was observed with the TRAF, ARM, and C-terminal disordered region deletion variants, puncta signals could still be observed, suggesting these domains are not solely required. However, when the CC domain and the C-terminal disordered region were deleted together, the puncta could no longer be observed, suggesting that the CC domain is necessary for TC1b subcellular localization (Figure 5a,b).

The TRAF domains and the CC domain of TC1b are indispensable for its function

Since loss of the CC domain, but not the other domains, strongly impairs TC1b-YFP localization to puncta, we tested whether this variant was still functional. *p35S::TC1b-YFP* and truncation variants were transformed into the *tc1b-1 snc1* background for transgene complementation. Variants with deletions in the N- and C-terminal disordered regions could still enhance *snc1* dwarfism (Figure 5c). Consistent with this, these regions were not well conserved between TC1b homologs from different species, suggesting that they are not important for TC1b function (Figure S12). ARM domain deletion variants were only slightly impaired in function, suggesting that this domain is not fully required for TC1b function. Interestingly, the puncta localization appears to be important for TC1b function, as loss of the CC domain prevented complementation. Lastly, although the four TRAF domains were not essential for puncta localization, they seemed to be essential for protein function as no complementation was observed. Overall, only the TRAF and CC domains appear to be essential for TC1b function.

Identification of TC1b interactors

Some TRAF domain proteins work together with or inhibit TRAF-E3s through TRAF–TRAF associations (Qi et al., 2017). In another example, mammalian TRAF1, a TRAF domain protein that lacks the really interesting new gene (RING) E3 ligase domain, can function together with other TRAF-E3 proteins (like TRAF2) (Xie, 2013;Park, 2018). Thus, we attempted to identify potential TRAF domain proteins and other interactors that may mediate oligomerization, localization, or function of TC1b. Immunoprecipitation coupled with mass spectrometry (IP-MS) was carried out using TC1b-FLAG-expressing plants in the *tc1ab-1 snc1* background. Since these TC1b-FLAG overexpression lines have severely dwarfed phenotypes, they likely possess a significantly different proteome than WT or GFP overexpression lines (Figure 6a,b). A more comparable control line was generated where a stop codon was inserted between the *TC1b* gene and the FLAG epitope. This TC1b^{STOP}-FLAG control line closely resembles the TC1b-FLAG lines in morphology (Figure 6a,b). TC1b-FLAG could be enriched upon co-IP of tissue from the tagged lines, but not control lines (Figure 6c). Furthermore, the enriched TC1b-FLAG could be detected on a silver-stained SDS-PAGE gel (Figure 6d). Thus, TC1b-FLAG was successfully IPed.

By analyzing peptides from the IP-MS experiment, we identified potential candidate interactors that may function with TC1b (Table 1). Peptides from TC1b were the most abundantly detected peptides (Table 1), confirming that the IP was successful. Interestingly, many ribosomal components and proteasomal components were identified to be specifically enriched in TC1b-FLAG samples (Table 1), suggesting that TC1b may function in these complexes.

DISCUSSION

TC1b as a novel TRAF protein involved in plant immunity

In our study, we revealed that TC1b, but not the close homolog TC1a, is required for *snc1* autoimmunity (Figure 1, Figure S6). According to our epistasis analysis, TC1b is not a general downstream regulator of NLRs or PRRs or a general regulator of SNC1 homeostasis (Figures 3 and 4). TC1b likely also does not directly work in a complex with SNC1 or downstream of ADR1-L2 (Figure 4), suggesting that it may play a more indirect role in SNC1 activation or regulation.

Multiple plant TRAF domain proteins have been previously reported to be involved in immunity (Qi et al., 2022). The deubiquitinating enzymes UBIQUITIN-SPECIFIC PROTEASE 12 (UBP12) and UBP13, which possess an N-terminal TRAF domain, are negative regulators of bacterial resistance against *P.s.t.* DC3000 in Arabidopsis and of the hypersensitive response (HR) elicited by transgenic expression of PRR Cf-9 with Avr9 in tobacco (*N. benthamiana* and *N. tabacum*) (Ewan et al., 2011). In tomato (*Solanum lycopersicum*), SEVEN IN ABSENTIA 3 (*Sl*SINA3), a TRAF-RING E3 ligase, ubiquitinates and mediates degradation of the defense-related transcription factor NAM, ATAF1,2, CUC2 1 (*Sl*NAC1) (Miao et al., 2016). Interestingly, co-expression of

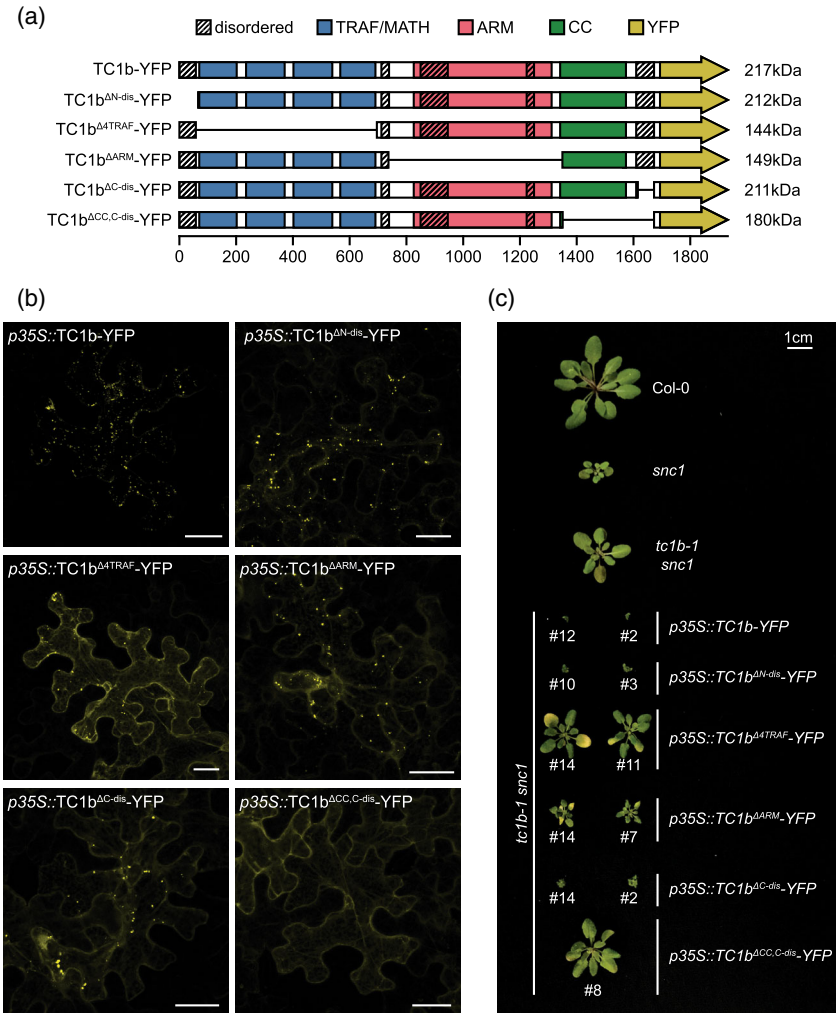

Figure 5. TC1b puncta localization relies on the CC domain, and TC1b function requires the CC and four TRAF domains.
(a) Scale diagram of truncations of TC1b-YFP made for domain deletion analysis. Domains are color-coded. Predicted sizes of truncated proteins are noted on the right in kDa. Internal domain deletions are represented with a horizontal line. Numbers on the axis show relative protein length in amino acids.
(b) Confocal laser scanning microscopy images of *Nicotiana benthamiana* epidermal cells expressing *35S::TC1b-YFP* or truncations. Images are Z-stack projections. Bars = 30 μm.
(c) Morphology of 3.5-week-old soil-grown plants of the indicated genotypes. Scale bar is 1 cm. *TC1b-YFP* and truncated variants were transformed into the *tc1b-1 snc1* background for transgene complementation.

*Sl*SINA1/2/3/5/6 can suppress the HR elicited by transient expression of various autoactive NLRs in tobacco, whereas independent expression of *Sl*SINA4 can cause HR, suggesting they may differentially regulate NLR-mediated immunity (Miao et al., 2016; Wang et al., 2018). Finally, RESTRICTED TEV MOVEMENT 3 (RTM3) is a CC domain-containing TRAF protein that prevents the long-distance movement of potyviruses through an unclear mechanism (Cosson et al., 2010). The finding that TC1b contributes to SNC1-mediated responses provides a new example of a TRAF domain protein that is involved in immunity.

The TRAF proteins MUSE13 and MUSE14 are negative regulators of SNC1 defense (Huang et al., 2016), whereas TC1b plays an opposite role. It is possible that one regulator may negatively regulate the other to prevent its activity. This could occur through TRAF–TRAF interactions as both MUSE13/14 and TC1b have TRAF domains that may hetero-oligomerize. Interestingly, the TRAF domains of TC1a/b appear to be phylogenetically related to those from MUSE13/14-like proteins (Figure S1). However, MUSE13/14 were not identified in the IP-MS data, suggesting that it does not interact with TC1b-FLAG, it is quickly degraded during IP, and/or it is lowly expressed. MUSE13/14 is targeted by the E3 ligase complex $SCF^{SNIPER4}$ for degradation, suggesting that its native protein level may be low (Huang et al., 2018). MUSE13/14 is a regulator of SNC1 homeostasis, whereas TC1b does not seem to affect SNC1 protein levels (Figure 4), further suggesting these regulators work differently. Of note, one study reported

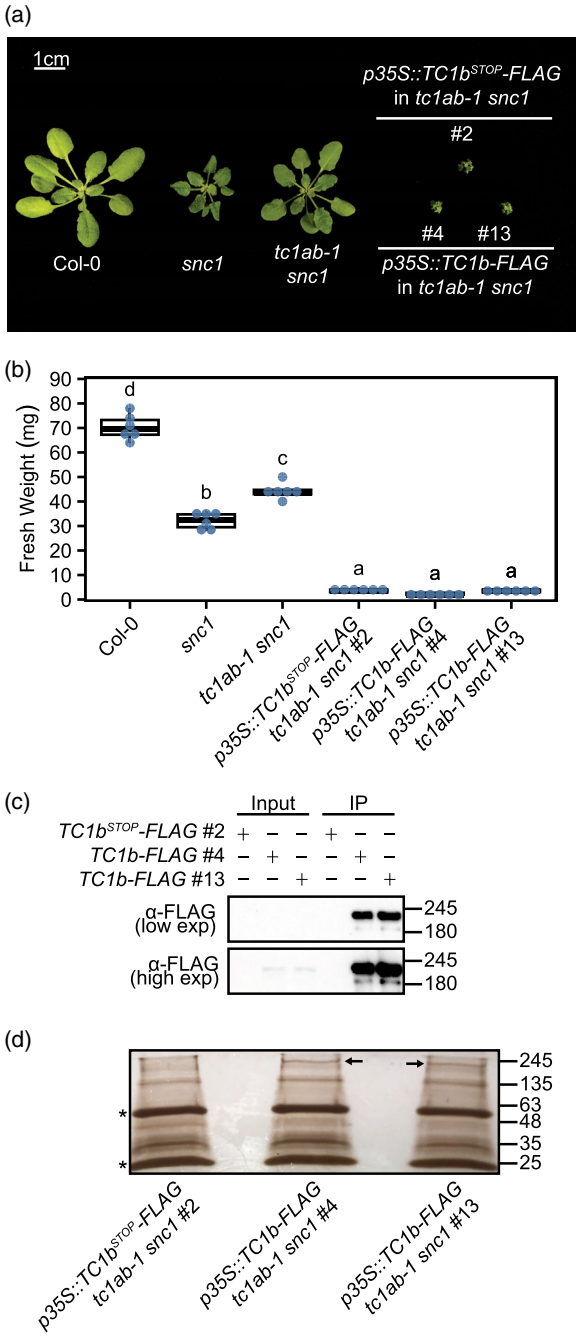

Figure 6. Immunoprecipitation of TC1b-FLAG. (a) Morphology of 3.5-week-old soil-grown plants of the indicated genotypes. Bar, 1 cm. (b) Quantification of fresh weight of plants from (a). Box plots are overlaid with dot plots of raw data points ($n = 6$). Means not sharing any letter are significantly different ($P < 0.05$), determined using one-way ANOVA with the post-hoc Tukey HSD test. (c) Western blot analysis of immunoprecipitated TC1b-FLAG from Arabidopsis transgenic lines, compared with non-tagged controls. Approximate protein sizes are marked on the right in kDa.Both low and high exposure blot is shown. (d) Silver-stained SDS-PAGE gel containing immunoprecipitated TC1b-FLAG from Arabidopsis transgenic lines. Arrows show the bait protein. Asterisks denote high-abundance proteins that were excised and sequenced separately. The data from high- and low-abundance bands were combined upon data analysis. Approximate protein sizes are marked on the right in kDa.

that MUSE13/14 interacts with the TRAF domain-containing RING-E3 ligases SEVEN IN ABSENTIA OF ARABIDOPSIS THALIANA 1/2/6 (SINAT1/2/6) and regulates the degradation of the autophagy-related proteins AUTOPHAGY PROTEIN 6 (ATG6) and ATG13 (Qi et al., 2017; Qi et al., 2020). It is possible that TC1b functions through interacting with SINATs or other TRAF proteins, and their absence in the IP-MS dataset may be explained by low prey protein abundance (due to their ubiquitination/degradation function) or protein extraction conditions.

Potential mechanism for the suppression of *snc1* phenotypes by loss of TC1b

The finding that TC1b does not contribute to the autoimmunity of any other tested autoimmune mutants besides *snc1* suggest that TC1b is not a general regulator (Figure 3). This is in contrast to many of the previously identified regulators important for *snc1* autoimmunity that contribute to general immunity such as the nuclear pore component MOS7/NUP88 and MOS4-associated complex components (Cheng et al., 2009; Monaghan et al., 2009; Palma et al., 2007; Xu et al., 2011; Xu et al., 2012; Zhang et al., 2005). TC1b also likely does not contribute to pathways of other known SNC1 protein homeostasis regulators like the SNC1-targeting E3 ligase CPR1 (Cheng et al., 2011; Gou et al., 2012) or the NLR-targeting E3 ligases SNIPER1/2 (Wu et al., 2020).

Although we failed to detect these proteins in our IP-MS experiments, there are several known regulators that affect SNC1 function but are not involved in SNC1 protein homeostasis. One potential group of regulators that TC1b may function with is the bHLH84 transcription factor family. Similar to TC1b loss-of-function mutants, *snc1* autoimmunity is partially blocked in triple mutants of the *bHLH84* family members (Figure 1) (Xu et al., 2014). In addition, overexpression of both TC1b and bHLH84 family members results in enhanced dwarfism in *snc1* (Figure 2) (Xu et al., 2014). Importantly, neither TC1b nor bHLH84 affects SNC1 protein levels (Figure 4) (Xu et al., 2014). It is possible that TC1b and bHLH84 members function together or that TC1b affects the expression or homeostasis of bHLH84 members or vice versa.

TC1b could also function with TOPLESS/TOPLESS-RELATED (TPL/TPR) proteins, transcriptional co-repressors which have been shown to be required for *snc1* autoimmunity (Zhu et al., 2010). The knockout and overexpression phenotypes of *TC1b* and *TPR* are similar, and *SNC1* expression is not significantly different in *TPR* mutant plants (Figures 1 and 2) (Zhu et al., 2010). Although TPL/TPR were suggested to be required for downstream transcriptional signaling, it is also possible that TPL/TPR may be SNC1 guardees since TPR1 can associate with SNC1. TC1b could function through TPL/TPR1 via various mechanisms. TPR1 is known to be SUMOylated, which inhibits its repressor

Table 1 Potential TC1b interactors from IP-MS analysis

Locus	Protein name/description	MW (Da)	Ctrl # queries	IP # queries	# Ctrl samples matched	# IP samples matched
AT2G25320	TC1b	187558	2	2895	2	4
AT3G07110	Ribosomal protein L13 family protein	23451	11	41	2	4
AT5G02870	RIBOSOMAL LARGE SUBUNIT 4 (RPL4)	44694	4	26	1	4
AT3G24830	Ribosomal protein L13 family protein	23444	0	20	0	2
AT5G10360	RIBOSOMAL PROTEIN SMALL SUBUNIT 6B (RPS6B)	28144	0	19	0	3
AT5G09590	HEAT SHOCK COGNATE (HSC70-5)	72946	0	17	0	3
AT1G07320	RIBOSOMAL PROTEIN L4 (RPL4)	30540	3	17	1	4
AT2G47610	Ribosomal protein L7Ae/L30e/S12e/Gadd45 family protein	29111	0	14	0	2
AT2G07698	ATPase, F1 complex, alpha subunit protein	85879	0	13	0	2
AT1G54270	Eukaryotic initiation factor 4A-2 (EIF4A-2)	46733	0	12	0	2
AT3G52580	Ribosomal protein S11 family protein	16228	0	12	0	2
AT1G02500	S-ADENOSYLMETHIONINE SYNTHETASE 1 (SAM1)	43131	0	11	0	2
AT4G18100	Ribosomal protein L32e	15493	1	10	1	4
AT1G02780	EMBRYO DEFECTIVE 2386 (emb2386)	24591	0	9	0	3
AT1G18540	Ribosomal protein L6 family protein	26136	0	8	0	2
AT4G34200	EMBRYO SAC DEVELOPMENT ARREST 9 (EDA9)	63286	0	7	0	3
AT3G56910	PLASTID-SPECIFIC 50S RIBOSOMAL PROTEIN 5 (PSRP5)	16351	1	7	1	4
AT1G35680	CHLOROPLAST RIBOSOMAL PROTEIN L21 (RPL21C)	24024	0	5	0	4
AT5G65220	PLASTID RIBOSOMAL PROTEINS OF THE 50S SUBUNIT 29 (PRPL29)	19365	0	5	0	3
AT3G13300	VARICOSE (VCS)	145630	0	5	0	3
AT5G02450	60S ribosomal protein L36-3	12182	0	4	0	4
AT1G09090	RESPIRATORY BURST OXIDASE HOMOLOG B (RBOHB)	96329	0	4	0	4
AT1G36240	Ribosomal protein L7Ae/L30e/S12e/Gadd45 family protein (RPL30A)	12310	0	4	0	4
AT5G23540	Mov34/MPN/PAD-1 family protein (RPN11)	34332	0	4	0	3
AT3G08940	LIGHT HARVESTING COMPLEX PHOTOSYSTEM II (LHCB4.2)	24986	0	4	0	3
AT5G58330	Lactate/malate dehydrogenase family protein	48286	0	4	0	3
AT5G42570	B-cell receptor-associated 31-like protein	28551	0	4	0	3
AT3G01370	CRM FAMILY MEMBER 2 (CFM2)	114527	0	4	0	3
AT4G24820	26S proteasome regulatory subunit Rpn7	44254	0	3	0	3
AT3G46440	UDP-XYL SYNTHASE 5 (UXS5)	38365	0	3	0	3
AT2G26080	GLYCINE DECARBOXYLASE P-PROTEIN 2 (GLDP2)	113703	0	3	0	3

Top candidate proteins that interact with TC1b are listed. Columns state the molecular weight (MW), total number of queries for control and IP samples, and the number of control and IP samples that detected each protein. Blue – TC1b, magenta – ribosomal proteins, green – proteasomal proteins, grey – other proteins.

activity (Niu et al., 2019). In addition, TPR2 and TPR3 are negative regulators of *SNC1*, potentially by competing with TPR1 for SNC1 binding (Garner et al., 2021). TC1b could potentially interfere with or activate these processes.

Another potential mechanism is that TC1b may work with MUSE1/2, RING-type E3 ubiquitin ligases, or with SIDEKICK SNC1 1/2/3 (SIKIC1/2/3), SNC1-related TNLs that were previously reported to be targeted by MUSE1/2 for degradation (Dong et al., 2018). Loss of both MUSE1 and MUSE2 results in severe dwarfism that is dependent on SNC1, whereas overexpression of MUSE1 can fully suppress *snc1* phenotypes. TC1b could potentially contribute to turnover or inactivation of MUSE1 and/or MUSE2, thus suppressing *snc1* phenotypes. Alternatively, TC1b may directly promote the stability or accumulation of the SIKICs.

Implications of TC1b protein domains

The TC1b TRAF domains likely serve as scaffolds, similar to mammalian TRAF proteins. Evidence from mammalian TRAF structures shows that TRAF–TRAF interactions are mediated through extensive interfaces, and TRAF–interactor/receptor interactions are mediated through a shallow minimal interface (Park, 2018; Park et al., 1999). Presumably, the TC1b TRAF domains mediate both intramolecular TRAF–TRAF interaction between its domains and intermolecular TRAF–TRAF

interactions to form larger TRAF complexes similar to mammalian trimeric complexes (Figure 4d) (Park, 2018). These larger complexes could consist of homo-oligomers, hetero-oligomers (for example with TC1a, TRAF-BTBs, or SINA/SINATs), or both. It is unclear why TC1b possesses four TRAF domains. Some multi-TRAF domain proteins are also found in the genomes of carrot (*Daucus carota*) and *Caenorhabditis elegans* (e.g., MATH-4, MATH-26, MATH-28, MATH-42) (Figure S1). It is possible that the larger number of TRAF domains allows for recruitment of more units of a putative interactor. Two scenarios for TC1b TRAF function can be imagined. TC1b could bind to previously oligomerized receptors/binding partners through the TRAF domains to mediate downstream signaling through its C-terminal domains (similar to the mammalian TRAF model). Alternatively, the signal transduction mechanism may be similar to the NLR resistosome model, where oligomerized TRAF-mediated recruitment of multiple interactor units by TC1b results in their induced proximity, oligomerization, and activation.

Since TC1b does not have E3 ligase domains, the ARM and CC domains provide additional functionality. Our results indicate that the CC domain is required for the puncta localization (Figure 5). CC domains can form trimeric or dimeric coils through protein–protein interactions. Long coils such as the one in TC1b may function as a molecular spacer, a molecular tether, or a scaffold for protein complex assembly (Gillingham & Munro, 2003; Truebestein & Leonard, 2016). Because the C-terminal end of TC1b is a short, disordered region rather than a structural domain, it is unclear how TC1b may bind a distal protein as part of a spacer or tether. Alternatively, the disordered region may be a ligand bound by a receptor-type protein or may be an anchor to attach to an unknown membrane component or protein complex.

The ARM domain is a common binding domain found in various proteins, including E3 ligases and alpha-importins (Mudgil et al., 2004; Wirthmueller et al., 2013), and could interact with many different types of substrates. The ARM domain potentially connects its ligand to the interactor bound by the TRAF domain or acts as an intramolecular regulator.

Implications of TC1b localization to puncta

It is unclear whether TC1b foci are known or novel structures. Further colocalization experiments, particularly with markers for membraneless organelles, may provide clues for its function. Interestingly, the wheat (*Triticum aestivum*) TRAF-BTB protein *Ta*MAB2 localizes to cytoplasmic foci in Arabidopsis protoplasts, and overexpression of *Ta*MAB2 leads to growth defects resembling autoimmune mutants (Bauer et al., 2019). In addition, the maize (*Zea mays*) TRAF-BTB *Zm*MAB1 localizes to speckles in the nucleus and cytoplasm of tobacco suspension cells, which is dependent on the cell cycle stage (Juranič et al., 2012). Lastly, the TRAF-CC protein RTM3 localizes to puncta in transiently transformed onion (*Allium cepa*) epidermal cells. Consistent with our study, this localization is prevented in a variant containing a mutation in the CC domain, further supporting the importance of CC domains for puncta localization (Cosson et al., 2010).

The additional SNC1 regulators SUPPRESSOR OF RPS4-RLD 1 (SRFR1) and TATA-BINDING PROTEIN-ASSOCIATED FACTOR 15B (TAF15b) localize to cytoplasmic puncta. SRFR1 is a negative regulator of ETI and is involved in the regulation of NLRs like SNC1 (Kim et al., 2010; Li et al., 2010). SRFR1 can localize to cytoplasmic puncta when transiently expressed in tobacco (Kwon et al., 2009). SRFR1 can also interact with SNC1 and RPS4 specifically in the cytoplasmic microsomal fraction (Kim et al., 2010) and can colocalize with EDS1 in cytoplasmic puncta (Bhattacharjee et al., 2011). TAF15b is an RNA-binding protein required for *snc1* autoimmunity (Dong, Meteignier, et al., 2016) and can localize to puncta-like RNA-processing bodies (p-bodies). Potentially, TC1b may work in a complex with these components to regulate SNC1, although such a hypothesis is not supported by our IP-MS results.

TRAF proteins in plants and animals

Immune receptors are used by both plants and animals as a common tool to recognize the presence of pathogens and activate downstream responses to handle pathogen threats. Compared with mammals, NLR families are expanded in many plant lineages and have large interspecific and intraspecific diversity (Barragan & Weigel, 2021). Many NLRs are encoded tandemly and/or in clusters, which is thought to mediate rapid diversification and adaptation under evolutionary pressure (Hulbert et al., 2001; Jacob et al., 2013; Meyers et al., 2003; Michelmore & Meyers, 1998). Similar to NLR genes, plant TRAF genes are frequently tandemly encoded, possibly to mediate adaptation to external challenges. Indeed, RTM3, a viral resistance protein, is encoded in a large 24-gene cluster of TRAF genes on Arabidopsis chromosome 3 (Figure S3) (Cosson et al., 2010), suggesting that genes in this cluster may have evolved to handle pressure from viruses. However, the TRAF gene clusters do not appear to correlate with clusters of NLRs or PRRs. Beyond plants, TRAF gene clustering is also found in other species. For example, 50 MATH genes are clustered together on chromosome 2 in *C. elegans* (Thomas, 2006). The biological significance of TRAF gene clustering awaits future analysis.

EXPERIMENTAL PROCEDURES

Plant growth conditions

Plant care and growth conditions were previously described (Ao et al., 2021). A temperature-controlled growth room was used to grow plants at 22°C under long-day (16 h light/8 h dark) conditions unless otherwise specified. Light was provided at an intensity of

approximately 100 μmol m^{-2} sec^{-1} from fluorescent bulbs. Severely dwarfed plants were grown in a 28°C chamber to suppress autoimmunity and yield seeds. For cold-induced autoimmune mutants, plants were grown in a 16°C growth room under short-day conditions or a 10°C chamber under constant light for the indicated times. Prior to planting, seeds were surface-sterilized with 15% bleach or chlorine gas and stratified for at least 48 h at 4°C in the dark. Seeds were sown on autoclaved Sunshine® Mix #4 soil (Sun Gro® Horticulture, Agawam, MA, USA) or on half-strength Murashige–Skoog medium (PhytoTech Labs, Lenexa, KS, USA) supplemented with 0.5% sucrose and 3 g L^{-1} Phytogel™ (½ MSA) and adjusted to pH 5.6.

Plasmid construction

Constructs for px-rb, GFP-2HA-TurboID, and SNC1-FLAG were described previously (Nelson et al., 2007; Wu et al., 2022; Xu et al., 2014). Two different CRISPR constructs were made. First, an sgRNA and ubiquitin promoter-driven Cas9 expression system (psgR-Cas9-At) that was previously described (Mao et al., 2013) was inserted into *pGreenII0229*. Annealed oligonucleotides containing sgRNA1 were cloned into *pGreenII0229-pAtU6-sgRNA-pAtUBQ-Cas9-tUBQ* using *Bbs*I sites. A second construct targeting the entire TC1a/b locus was generated using an egg cell Cas9 expression system (Wang et al., 2015; Xing et al., 2014). Two sgRNAs (sgRNA2/3) were introduced into the CRISPR binary vector *pBEE401E* using *Bsa*I sites according to previously published protocols (Wang et al., 2015; Xing et al., 2014). CRISPR-PLANT v2 and CRISPR-P v2.0 were used to help select sgRNAs (Liu et al., 2017; Minkenberg et al., 2019). Cas-OFFinder was used to check for sgRNA off-target regions (Bae et al., 2014). All sgRNAs are highly specific, with potential off-target sites containing at least four bp mismatches or a 1-bp DNA/RNA bulge (Table S5).

For overexpression, co-IP, and IP-MS analysis, genomic *TC1b* (with and without a stop codon) was cloned into constitutive expression vectors *pBasta-35S::3FLAG* and *pBasta-35S::2HA-TurboID* using *Dra*III sites. *pBasta-35S::SNC1-2HA-TurboID* was generated by cloning genomic *SNC1* into *35S::2HA-TurboID* using *Dra*III sites. For full-length and truncated *TC1b* constructs used for confocal microscopy, genomic fragments containing *TC1b* or truncation variants were cloned into *pBasta-35S:YFP* using *Dra*III sites. Overlap extension PCR was used for internal domain deletion constructs. For the native promoter-driven *TC1b-2HA-GFP* construct used for microscopy, a genomic fragment containing *TC1b* and an upstream approximately 800-bp sequence was cloned into *pBasta-2HA-GFP* using *Kpn*I and *Pst*I sites.

For colocalization analysis, *pUBQ10::mCherry-RabF2a*, *pUBQ10::mCherry-RabG3c*, and *pUBQ10::mCherry-RabA1g* were cloned from Wave 7R, Wave 11R, and Wave 129R lines described previously (Geldner et al., 2009). These fragments were used to regenerate *mCherry* constructs by replacing the *pUBQ10::EYFP-RabE1d* cassette in the Wave 27Y construct using *Eco*RI and *Not*I sites. Genomic *ATG8e* and *RBP47B* fragments were cloned from WT plants and used to replace the *RabF2a* fragment in the *pUBQ10::mCherry-RabF2a* construct using *Dra*III sites. All cloning primers used are listed in Table S4.

Plant materials, generation of mutant and transgenic plants

All Arabidopsis plants used were in the Col-0 background. The SALK_103885C (*tc1a-1*) and CS356847 (*tc1b-1*) T-DNA lines were obtained from the Arabidopsis Biological Resource Centre (ABRC). These lines were crossed with *snc1* to generate double mutants, which were verified by PCR using T-DNA-flanking primers (Table S4). Many of the other mutant and transgenic lines (*snc1*, *chs1-2*, *chs2-1*, *chs3-2D*, *mekk1-5*, *snc2-1D*, *eds1-2*, *agb1-2*, *fls2c efr-1 cerk1-2*, *ADR1-L2*^{D484V}) were previously described (Aarts et al., 1998; Bi et al., 2011; Bjornson et al., 2014; Gimenez-Ibanez et al., 2009; Huang et al., 2010; Li et al., 2001; Roberts et al., 2013; Ullah et al., 2003; Wang et al., 2013; Zhang et al., 2003; Zhang et al., 2010). To generate double mutants for epistasis, mutants were crossed with *tc1b-1*, and the autoimmune locus was fixed first. Double mutants were confirmed by PCR. Genotyping PCR primers are listed in Table S4.

Binary constructs carrying transgenes were transformed into *Agrobacterium tumefaciens* GV3101 using electroporation. Transgenic lines were generated using *Agrobacterium*-mediated floral-dip transformation (Clough & Bent, 1998). To select for transgenic plants on soil, 100 mg L^{-1} Basta® (glufosinate-ammonium) was sprayed. Generally, at least 20 individual T1 lines were followed, and lines with a difference in phenotype, single-copy insertions, and observed protein expression were kept for further analysis.

For screening CRISPR/Cas9-mutagenized plants, enhancers and suppressors identified in the T1 or T2 generations were PCR-genotyped using deletion-flanking primers at the target locus to identify potential deletions. For promising candidates with potential SNPs, the targeted region was amplified by PCR. Deletion and putative SNP-containing PCR fragments were sent for Sanger sequencing through a commercial service (Psomagen Inc., Rockville, MD, USA). Homozygous *tc1ab-1 snc1* and *tc1ab-2 snc1* plants were recovered using this process and crossed with WT to obtain single *tc1ab-1* and *tc1ab-2* mutants. *tc1ab-3 snc1* to *tc1ab-6 snc1* were recovered from screening T1 CRISPR lines that carried deletions. *snc1 eds1-25* was generated by transforming a previously described *EDS1a/b*-targeting CRISPR construct (Tian et al., 2021) into *snc1* and screening for deletions by PCR. The *eds1-25* allele contains a 2635-bp deletion between *EDS1a* and *EDS1b* (Figure S8a,b). *tc1b-1 snc1 eds1-25* and *TC1-FLAG #10 snc1 eds1-25* lines were generated by crossing. Triple homozygous lines were verified by PCR genotyping and non-segregation of herbicide resistance. Genotyping primers are listed in Table S4.

Infection assays

For *H.a.* Noco2 infection, spores in H_2O (10^5 spores mL^{-1}) were sprayed on 14-day-old soil-grown seedlings and allowed to grow in a humid chamber (12 h light/12 h dark, 18°C) for 7 days. A light microscope and a hemocytometer were used to quantify spores 7 days after inoculation. For *P.s.t.* infections, plants were grown on soil in a climate-controlled growth chamber under an 8 h light/16 h dark photoperiod. Leaves of 4-week-old plants were infiltrated with the specified bacterial strains at the indicated OD_{600} using a blunt-end syringe. Leaf discs from infected leaves were collected at 0 and 3 days post-infiltration. Bacterial titers were quantified by plating serial dilutions on LB plates with appropriate antibiotics.

Total protein analysis

First, 50–100 mg of frozen plant tissue per sample was ground to a fine powder using glass beads and a Precellys tissue homogenizer (Bertin Instruments, Montigny-le-Bretonneux, France). Total protein was extracted using extraction buffer (100 mM Tris–HCl pH 8.0, 0.1% SDS, 2% β-mercaptoethanol), added at a 1:1 ratio. High-speed centrifugation (21 130 ***g*** for 10 min) was used to remove cell debris. Samples were mixed with SDS-PAGE sample buffer, boiled for 10 min at 95°C, resolved on 6%, 8%, or 10% SDS-PAGE gels, and transferred to nitrocellulose membranes. Immunoblot analysis was completed using standard protocols. Antibodies and dilutions are listed in Table S7.

Turbo-ID proximity labeling and co-IP assays

Nicotiana benthamiana plants were infiltrated with construct-carrying *Agrobacterium* cultures. For Turbo-ID experiments, plants were infiltrated with 100 μM of biotin after 48 h and incubated for 1–2 h. Around 2 g of tissue per sample were then harvested and frozen in liquid nitrogen. Co-IP was performed following previously described protocols (Xu et al., 2015) with minor modifications. Frozen tissue was ground using a mortar and pestle or using glass beads and a benchtop homogenizer (BeadBug™, Benchmark Scientific Inc., Sayreville, NJ, USA). Total protein was extracted using co-IP buffer (100 mM Tris–HCl pH 7.5, 150 mM NaCl, 1 mM EDTA, 10% glycerol, 2% polyvinylpolypyrrolidone [PVPP], 10 mM DTT, 0.15% NP-40, protease inhibitor cocktail [no. 11836170001; Sigma-Aldrich, St. Louis, MO, USA], 1 mM PMSF). High-speed centrifugation at 21 130 ***g*** for 10 min was used to remove cell debris. The supernatant (input) was incubated together with anti-FLAG M2 Affinity gel agarose beads (A2220; Sigma-Aldrich) at 4°C for 2–3 h with gentle agitation. The beads, along with the IPed proteins, were collected through gentle centrifugation, washed three times with fresh co-IP buffer without PVPP, mixed with SDS-PAGE sample buffer, and boiled for 10 min at 95°C. Standard Western blot protocols were used to visualize proteins. Antibodies and dilutions are listed in Table S7.

Mass spectrometry analysis

First, 14-day-old seedlings grown on ½ MSA were harvested and frozen in liquid nitrogen. Two technical replicates were collected for each of the three genotypes (two TC1b-FLAG lines and one TC1b^{STOP}-FLAG line), resulting in six samples. Co-IP was carried out as described above. A previously described protocol (Ao et al., 2021) was followed for sample preparation and MS analysis with minor modifications. Matches that met one of the following criteria were considered top hits: (i) not identified in control samples and found in at least three of four IP samples; (ii) not identified in control samples and found in two IP samples with at least three unique peptides per sample; or (iii) identified in at least one of two control samples and all four IP samples, with average peptide levels in IP samples being at least 3 times as high as in control samples. The raw unfiltered IP-MS hits are listed in Table S8.

Gene expression analysis

For analyzing flg22-induced gene expression, 12-day-old seedlings grown on ½ MSA were sprayed with 1 μM flg22 or H_2O and collected after 4 h. A plant RNA extraction kit (Bio Basic, Markham, Ontario, Canada; Cat#BS82314) and TRIzol were used to extract total RNA. RNA (1 μg per sample) was reverse-transcribed using the OneScript™ cDNA Synthesis Kit (ABM, Richmond, British Columbia, Canada). cDNA and cDNA-specific primers were mixed with SYBR premix from a commercial kit (TaKaRa, Kusatsu, Japan, Cat#RR82LR) according to the manufacturer's recommendations, and qPCR was completed using a CFX96 Real-Time PCR machine (Bio-Rad Laboratories, Hercules, CA, USA). Melting curve analysis was conducted to ensure single products were amplified. *ACTIN7* was used to normalize expression values. Primers used are listed in Table S4.

Confocal microscopy

To image water-mounted *A. thaliana* and *N. benthamiana* leaf discs, a Leica TSC-SP5 confocal laser scanning microscope with a 20×/0.70 objective (PL APO, CS) or a Leica TSC SP8 Falcon confocal laser scanning microscope with a 20×/0.75 objective (HCPL APO CS2) was used. YFP and GFP were excited at 514 nm and 488 nm, respectively, by an argon laser line or a pulsed white light laser. mCherry was excited at 561 nm by a diode-pumped solid-state (DPSS) laser. HyD detectors were used to detect emitted fluorescence at 525–560 nm for YFP, 500–540 nm for GFP, and 580–620 nm for mCherry. A PMT detector was used to detect chlorophyll autofluorescence at 740–770 nm. Images were sequentially scanned. ImageJ was used to prepare images, generate maximum projections, and merge channels (Rueden et al., 2017).

Bioinformatics and generation of gene and protein diagrams

Percent identity and similarity were computed using EMBOSS Needle (Madeira et al., 2019). Protein domain information and annotation data were either gathered from InterPro through the REST web service client or through UniProt (Jones et al., 2014; Mitchell et al., 2019; UniProt Consortium, 2019). Intrinsically disordered region predictions were obtained from MobiDB-lite and D^2P^2 (Necci et al., 2020; Oates et al., 2013). Gene and protein diagrams and data graphs were prepared using the gggenes, ggplot2, and tidyverse packages in R (R Core Team, 2019; Wickham et al., 2019).

Data acquisition for phylogenetic analyses

For the analysis of TRAF domain phylogeny, proteins containing a TRAF domain (accession numbers: IPR008974, IPR002083, IPR018121, SSF49599) from 19 representative species were obtained from the InterPro annotation database. Protein sequences were filtered to remove duplicate alleles and isoforms programmatically and manually so that each gene locus was represented by a single protein sequence. All protein sequence accession information can be found in Table S1. Domain peptide sequences were extracted from protein sequences according to InterPro annotations of domain borders.

For the analysis of TC1a/b protein phylogeny, protein sequences of TC1a/b homologs from representative species were obtained from various sources (a full list of accessions and data sources can be found in Table S6) (Cunningham et al., 2022; Goodstein et al., 2012; Grigoriev et al., 2021; Li et al., 2018; One Thousand Plant Transcriptomes Initiative, 2019; Van Bel et al., 2018). Using the blastp utility on the source database websites, sequences significantly aligned with the *Chara braunii* TC1a/b protein sequence (UniProt accession: A0A388JUC4) were collected (E-value < 1.0E−10, default settings).

Multiple sequence alignment and phylogenetic inference

Protein sequences were aligned using an iterative refinement algorithm (L-INS-i) in a local installation of MAFFT version 7.480 (Katoh & Standley, 2013) accessed through Mesquite version 3.61+ (build 936) (Madison & Madison, 2019).

A model of sequence evolution was selected using the ModelFinder tool in IQ-TREE ver. 2.1.2 (Kalyaanamoorthy et al., 2017; Minh et al., 2020). A Jones amino acid exchange matrix with empirical amino acid frequencies and a discrete Gamma model of rate heterogeneity (JTT + F + G) was the best-fit model for both the domain and the protein alignments according to both AIC and BIC criteria and was used as the substitution model for the tree inferences. Using IQ-TREE, 30 and 50 independent maximum likelihood (ML) tree searches were done for the domain and protein phylogenies, respectively, to ensure a thorough search of the treescape and to increase the chances of finding better trees. The tree found with the best log-likelihood was used for further analysis. For the protein tree, the best ML gene tree was found more

than once in independent tree searches, suggesting that the number of replicates was sufficient. Branch supports for the domain and protein phylogeny were obtained through non-parametric bootstrapping in RAxML version 8.2.12 ($n = 300$) (Stamatakis, 2014) and IQ-TREE ($n = 500$), respectively. To determine whether the number of bootstrap replicates was sufficient for the protein phylogeny, the *a posteriori* bootstrap convergence analysis tool in RAxML was used (Pattengale et al., 2009). A distance-based criterion (-I autoMR) was used to test the convergence of majority-rules consensus trees, and the test suggested sufficient bootstrap replicates were performed.

A majority-rules consensus TC1a/b protein tree with a cut-off threshold of 0.75 was generated from the 500 bootstrap gene trees. A parsimony-based program, Notung version 2.9, was used for reconciliation of the non-binary protein tree and the binary species tree using the Resolve function (Durand et al., 2006). The species phylogeny of the species represented in the gene tree was based on the current consensus of eukaryote evolution (Burki et al., 2020; Leliaert et al., 2012; The Angiosperm Phylogeny Group et al., 2016). Phylogenetic trees were visualized using the R package ggtree (Yu, 2022).

Statistical analysis

Graph data are presented as box plots with the lower and upper hinges representing the first and third percentiles and the center line representing the median. Whiskers extend at most 1.5 × the interquartile range (IQR) from the lower and upper hinge to the smallest and largest values, respectively. Outliers are individually plotted and not linked by whiskers. Box plots are overlaid with dot plots representing data points. To determine statistical significance, one-way analysis of variance (ANOVA) was used, followed by Tukey's HSD test. Compact letter display is used to represent statistically significant differences. Groups not sharing any letters are significantly different ($P < 0.05$).

AUTHOR CONTRIBUTIONS

KA carried out the *tc* CRISPR/Cas9 reverse genetic screen, characterized the mutants, and performed most experiments; PFWR and SH performed confocal microscopy; LL performed the MS analysis; MW, VL, SC, and XL provided tools, materials, and expertise and analyzed data; XL supervised the project; KA wrote the manuscript draft and prepared figures; XL revised the manuscript. All authors provided input on the manuscript and approved the final version.

ACKNOWLEDGMENTS

We thank Dr. Jeff Dangl, Dr. Shuhua Yang, Dr. Cyril Zipfel, Dr. Jane Parker, Dr. Jian-Kang Zhu, and Dr. Qi-Jun Chen for the sharing of Arabidopsis mutant seeds and the CRISPR constructs. We thank Dr. Yanan Liu, Dr. Yuti Cheng, and Dr. Yuli Ding for modifying and optimizing the *pGreenII0229*-based CRISPR system and Dr. Zhongshou Wu for generating the *SNC1-2HA-TurboID* construct. We thank Dr. Gillian Dean and Dr. Elena Petutschnig for sharing materials for colocalization analysis. This study was financially supported by grants to XL from the Natural Sciences and Engineering Research Council (NSERC) Discovery program of Canada and the Canadian Foundation for Innovation (CFI) and scholarships to KA from the NSERC Graduate Scholarships – Master's Program, the Alexander Graham Bell Canada Graduate Scholarships – Doctoral Program, the NSERC Michael Smith Foreign Study Supplement Program, and the University of British Columbia Four-year fellowship program. PFWR and MW are supported by funding from the Deutsche Forschungsgemeinschaft (DFG) (research grant WI 3208/8-1). VL thanks the DFG for grants INST 186/824-1 FUGG and INST 186/1277-1 FUGG. Funding from NSERC-CREATE and the DFG to the International Research Training Group (IRTG 2172, PRoTECT) allowed for the collaborative research in this study.

CONFLICT OF INTEREST

The authors declare no conflicts of interest.

DATA AVAILABILITY STATEMENT

All relevant data can be found within the manuscript and its supporting materials. Materials generated in this study are available upon request.

SUPPORTING INFORMATION

Additional Supporting Information may be found in the online version of this article.

Figure S1. Phylogenetic tree of TRAF domains from selected species.

IQ-TREE-produced maximum likelihood tree (best out of 30 tree searches) inferred from amino acid alignment of TRAF domains from 19 diverse species. Bootstrap values (from 300 RAxML bootstrap replicates) are shown at nodes as colored points; branches with bootstrap support of over 70% are marked in red. A root was chosen based on parsimony. Tip labels are colored based on species groups (red, *A. thaliana*; green, Archaeplastida; black, Opisthokonta). Tip labels contain domain/protein information in the following order: the UniProt accession code from which the domain sequence originated, the order of the TRAF domain within the protein and the total number of TRAF domains in the protein (separated by a forward slash), the gene code and gene name (if available) for sequences from *A. thaliana*, a five-letter abbreviation for species from which the sequence originated, the protein classification (based on this phylogeny and/or based on the PANTHER classification system), the CRISPR deletion group in square brackets (genes chosen for CRISPR mutagenesis – see Table S3 for more details), and an asterisk for shorter (<75-aa) domains that may be incorrectly placed in the tree. The TRAF domain family is classified into subfamilies, which is correlated with the protein architecture (see Figure S2) and is highlighted by clade labels and shading. Clades to note include: species-specific TRAF domain expansions (*C. elegans*, *Papaver*, rice BPMs, Arabidopsis TRAF-CCs), mammalian immunity-related TRAF1–6, and the TC1a/b clade. See Table S1 for protein accessions, domain sequences, and other details.

Figure S2. Protein domain architecture of Arabidopsis TRAF domain proteins.

Domain architecture schematic of Arabidopsis TRAF domain proteins drawn to scale. Arabidopsis TRAF proteins and domain data were collected from the UniProt and InterPro databases. Domains are color-coded (see domain legend). A scale bar shows protein length in amino acids. Transcript names, gene names, and UniProt protein accession numbers are provided where available. The names of genes that were chosen for CRISPR mutagenesis are colored in red. A single representative isoform was chosen for each gene locus. Proteins are grouped into 11 classes according to previous publications, PANTHERdb classifications, and our own phylogenetic analysis (Figure S1). Domain name abbreviations: BTB,

broad-complex, tramtrack and bric a brac; BACK, BTB and C-terminal Kelch; USP, ubiquitin specific protease; USP-C, USP C-terminal; ICP0-b, ICP0-binding; Dis, disordered region; SP, signal peptide; PL, phospholipase-like; ING, inhibitor of growth; LUC, luciferase-like.

Figure S3. Chromosomal locations of Arabidopsis genes encoding TRAF domain-containing proteins.

Chromosome diagram showing genomic locations of genes encoding TRAF domain-containing proteins in Arabidopsis. In addition to AGI gene codes, gene names are provided (when available) in parentheses. The protein subfamily classification (from Figure S2) is also denoted. The group numbers in square brackets correspond to the groups of genes targeted in the CRISPR screen (see Table S3 for details). Selected candidate genes are colored red.

Figure S4. CRISPR reverse genetic screen for TRAF candidates.

A schematic describing the workflow of the genetic screen. CRISPR constructs were designed to target multiple closely related TRAF domain-containing proteins. Each construct was individually transformed into *snc1* plants using *Agrobacterium*-mediated floral-dip transformation. T1 plants were selected for the presence of the CRISPR transgene cassette and screened for suppressors or enhancers of the *snc1* morphology. If no candidates were identified in the T1 generation, plants were harvested and rescreened in the T2 generation. The targeted CRISPR region in the candidate enhancers or suppressors was sequenced to identify mutations. Confirmed suppressors and enhancers were further characterized.

Figure S5. Protein consequences of mutations in *tc1ab-1 snc1* and *tc1ab-2 snc1* lines.

Protein sequences of WT and mutant alleles of TC1a and TC1b are shown. Red font indicates the altered sequences due to frameshift.

Figure S6. Morphology of *tc1ab-3 snc1* to *tc1ab-6 snc1* lines.

(a) Morphology of 3.5-week-old soil-grown plants of indicated genotypes. Scale bar is 1 cm.

(b) Quantification of fresh weight of plants from (a). Box plots are overlaid with original data points ($n = 6$). Means not sharing any letter are significantly different ($P < 0.05$), determined using one-way ANOVA with the post-hoc Tukey HSD test.

Figure S7. Phylogenetic analysis of TC1a and TC1b protein homologs in selected plant species.

(a) Cladogram showing a reconciliated tree generated using NOTUNG (Durand et al., 2006) from a consensus maximum likelihood TC1a/b protein tree and a species tree. Inferred duplication events are denoted by a red label at nodes and inferred losses are denoted in tip labels with species name(s). The tree was rooted between Chlorophyta and Streptophyta clades.

(b) Table showing the prevalence of *TC1a* and *TC1b* in close relatives of *Arabidopsis thaliana*, along with a phylogenetic tree of species relationships. Information was obtained through the comparative genomics tools of Ensembl Plants (Cunningham et al., 2022).

(c) Number of Arabidopsis ecotypes that carry high-impact SNPs or indels in *TC1a* or *TC1b*. Information for the ecotype variations was obtained programmatically from the 1001 Genomes Project using their web services API (The 1001 Genomes Consortium, 2016).

Figure S8. The deletion of *EDS1a* and *EDS1b* in the *eds1-25* allele.

(a) Gene diagram of the *EDS1a/b* locus showing sites targeted by CRISPR sgRNA (vertical arrows) within the genes (horizontal arrows).

(b) *EDS1a/b* mutations in the *snc1 eds1-25* plants. Gene direction (horizontal arrow), PAM sequences (green text), sgRNA target sites (bold text), mutation sites (vertical arrow), sequences hidden for conciseness (//), and deleted bases (–) are marked. Deletion sizes of alleles are indicated in parentheses on the right. Sanger sequencing chromatograms are provided below the mutant allele sequence.

Figure S9. *TC1b-2HA-TurboID* overexpression can enhance *snc1* phenotypes.

(a) Morphology of 3.5-week-old soil-grown plants of the indicated genotypes. Scale bar is 1 cm.

(b) Quantification of fresh weight of plants from (a). Box plots are overlaid with dot plots of raw data points ($n = 6$). Means not sharing any letter are significantly different ($P < 0.05$), determined using one-way ANOVA with the post-hoc Tukey HSD test.

Figure S10. TC1b-YFP and TC1b-2HA-GFP are functional and localize to puncta.

(a, c) Morphology of approximately 3.5-week-old soil-grown plants of the indicated genotypes. Scale bar is 1 cm.

(b, d) Quantification of fresh weight of plants from (a) and (c), respectively. Box plots are overlaid with dot plots of raw data points ($n = 6$). Means not sharing any letter are significantly different ($P < 0.05$), determined using one-way ANOVA with the post-hoc Tukey HSD test.

(e, f) Confocal laser scanning microscopy images of *Nicotiana benthamiana* epidermal cells expressing *p35S::TC1b-YFP* (e) or *pTC1b::TC1b-2HA-GFP* (f). Images are Z-stack projections. Bars = 30 μm. The image overlays are a composite of the three channels.

Figure S11. TC1b-YFP does not colocalize with peroxisomal, endosomal, autophagosomal, or stress granule markers.

(a–f) Confocal laser scanning microscopy images of *Nicotiana benthamiana* epidermal cells expressing *p35S::TC1b-YFP* with various localization markers, including mCherry-SKL (px-rb), a peroxisome marker (a), mCherry-RabF2a (Wave 7R), a late endosome/multi-vesicular body marker (b), mCherry-RabA1g (Wave 129R), an endosome/recycling endosome marker (c), mCherry-RabG3c (Wave 11R), a late endosome marker (d), mCherry-ATG8e, an autophagosome marker (e), and mCherry-RBP47B, a stress granule marker (f). Bars = 30 μm. Images are single plane slices. Empty white arrows, TC1b-YFP puncta; filled white arrows, marker puncta. The image overlay is a composite of the two fluorescence channels.

Figure S12. Percent identity of protein residues between TC1b and homologs from other species.

The alignment used for the maximum likelihood phylogenetic tree underlying Figure S7a was visualized using Jalview (Waterhouse et al., 2009). Residue positions are shaded according to percentage of residues that agree with the consensus sequence. Only individual residues that are identical to the consensus residue are shaded. Shade intensity represents percent conservation above certain thresholds (see legend). Numbers on either side of the alignment describe the residue number of the particular sequence at that position. Domains (relative to Arabidopsis TC1b) are highlighted with colored boxes, corresponding to domains shown in Figure 1g. Accession numbers and further details can be found in Table S6.

Table S1. Protein accessions and data sources for the TRAF domain phylogenetic tree.

Table S2. Expression analysis of TRAF domain genes.

Table S3. Selected gene groups, construct design, and screening.

Table S4. Primers used in this study.

Table S5. Potential on- and off-target sites for CRISPR sgRNAs.

Table S6. Protein accessions and data sources for the TC1a/b phylogenetic tree.

Table S7. Antibodies and protein detection reagents used in this study.

Table S8. Unfiltered IP-MS hits.

REFERENCES

Aarts, N., Metz, M., Holub, E., Staskawicz, B.J., Daniels, M.J. & Parker, J.E. (1998) Different requirements for EDS1 and NDR1 by disease resistance genes define at least two R gene-mediated signaling pathways in Arabidopsis. *Proceedings of the National Academy of Sciences of the United States of America*, **95**, 10306–10311.

Albert, I., Hua, C., Nürnberger, T., Pruitt, R.N. & Zhang, L. (2020) Surface sensor systems in plant immunity. *Plant Physiology*, **182**, 1582–1596.

Ao, K., Tong, M., Li, L., Lüdke, D., Lipka, V., Chen, S. et al. (2021) SCFSNIPER7 controls protein turnover of unfoldase CDC48A to promote plant immunity. *The New Phytologist*, **229**, 2795–2811.

Bae, S., Park, J. & Kim, J.-S. (2014) Cas-OFFinder: a fast and versatile algorithm that searches for potential off-target sites of Cas9 RNA-guided endonucleases. *Bioinformatics*, **30**, 1473–1475.

Barragan, A.C. & Weigel, D. (2021) Plant NLR diversity: the known unknowns of pan-NLRomes. *Plant Cell*, **33**, 814–831.

Bauer, N., Škiljaica, A., Malenica, N., Razdorov, G., Klasić, M., Juranić, M. et al. (2019) The MATH-BTB protein TaMAB2 accumulates in ubiquitin-containing foci and interacts with the translation initiation machinery in Arabidopsis. *Frontiers in Plant Science*, **10**, 1469.

Bhattacharjee, S., Halane, M.K., Kim, S.H. & Gassmann, W. (2011) Pathogen effectors target Arabidopsis EDS1 and alter its interactions with immune regulators. *Science*, **334**, 1405–1408.

Bi, D., Johnson, K.C.M., Zhu, Z., Huang, Y., Chen, F., Zhang, Y. et al. (2011) Mutations in an atypical TIR-NB-LRR-LIM resistance protein confer autoimmunity. *Frontiers in Plant Science*, **2**, 71.

Bjornson, M., Benn, G., Song, X., Comai, L., Franz, A.K., Dandekar, A.M. et al. (2014) Distinct roles for mitogen-activated protein kinase signaling and CALMODULIN-BINDING TRANSCRIPTIONAL ACTIVATOR3 in regulating the peak time and amplitude of the plant general stress response. *Plant Physiology*, **166**, 988–996.

Branon, T.C., Bosch, J.A., Sanchez, A.D., Udeshi, N.D., Svinkina, T., Carr, S.A. et al. (2018) Efficient proximity labeling in living cells and organisms with TurboID. *Nature Biotechnology*, **36**, 880–887.

Burki, F., Roger, A.J., Brown, M.W. & Simpson, A.G.B. (2020) The new tree of eukaryotes. *Trends in Ecology & Evolution*, **35**, 43–55.

Cheng, Y.T., Germain, H., Wiermer, M., Bi, D., Xu, F., García, A.V. et al. (2009) Nuclear pore complex component MOS7/Nup88 is required for innate immunity and nuclear accumulation of defense regulators in Arabidopsis. *Plant Cell*, **21**, 2503–2516.

Cheng, Y.T., Li, Y., Huang, S., Huang, Y., Dong, X., Zhang, Y. et al. (2011) Stability of plant immune-receptor resistance proteins is controlled by SKP1-CULLIN1-F-box (SCF)-mediated protein degradation. *Proceedings of the National Academy of Sciences of the United States of America*, **108**, 14694–14699.

Clough, S.J. & Bent, A.F. (1998) Floral dip: a simplified method for agrobacterium-mediated transformation of Arabidopsis thaliana. *The Plant Journal*, **16**, 735–743.

Cosson, P., Sofer, L., Le, Q.H., Léger, V., Schurdi-Levraud, V., Whitham, S.A. et al. (2010) RTM3, which controls long-distance movement of potyviruses, is a member of a new plant gene family encoding a meprin and TRAF homology domain-containing protein. *Plant Physiology*, **154**, 222–232.

Cui, H., Tsuda, K. & Parker, J.E. (2015) Effector-triggered immunity: from pathogen perception to robust defense. *Annual Review of Plant Biology*, **66**, 487–511.

Cunningham, F., Allen, J.E., Allen, J., Alvarez-Jarreta, J., Amode, M.R., Armean, I.M. et al. (2022) Ensembl 2022. *Nucleic Acids Research*, **50**, D988–D995.

Dong, O.X., Ao, K., Xu, F., Johnson, K.C.M., Wu, Y., Li, L. et al. (2018) Individual components of paired typical NLR immune receptors are regulated by distinct E3 ligases. *Nature Plants*, **4**, 699–710.

Dong, O.X., Meteignier, L.-V., Plourde, M.B., Ahmed, B., Wang, M., Jensen, C. et al. (2016) Arabidopsis TAF15b localizes to RNA processing bodies and contributes to snc1-mediated autoimmunity. *Molecular Plant-Microbe Interactions*, **29**, 247–257.

Dong, O.X., Tong, M., Bonardi, V., El Kasmi, F., Woloshen, V., Wünsch, L.K. et al. (2016) TNL-mediated immunity in Arabidopsis requires complex regulation of the redundant ADR1 gene family. *The New Phytologist*, **210**, 960–973.

Dongus, J.A. & Parker, J.E. (2021) EDS1 signalling: At the nexus of intracellular and surface receptor immunity. *Current Opinion in Plant Biology*, **62**, 102039.

Durand, D., Halldórsson, B.V. & Vernot, B. (2006) A hybrid micro-macroevolutionary approach to gene tree reconstruction. *Journal of Computational Biology*, **13**, 320–335.

Duxbury, Z., Wang, S., MacKenzie, C.I., Tenthorey, J.L., Zhang, X., Huh, S.U. et al. (2020) Induced proximity of a TIR signaling domain on a plant-mammalian NLR chimera activates defense in plants. *Proceedings of the National Academy of Sciences of the United States of America*, **117**, 18832–18839.

El Kasmi, F. (2021) How activated NLRs induce anti-microbial defenses in plants. *Biochemical Society Transactions*, **49**, 2177–2188.

Ewan, R., Pangestuti, R., Thornber, S., Craig, A., Carr, C., O'Donnell, L. et al. (2011) Deubiquitinating enzymes AtUBP12 and AtUBP13 and their tobacco homologue NtUBP12 are negative regulators of plant immunity. *The New Phytologist*, **191**, 92–106.

Fang, X., Wang, L., Ishikawa, R., Li, Y., Fiedler, M., Liu, F. et al. (2019) Arabidopsis FLL2 promotes liquid-liquid phase separation of polyadenylation complexes. *Nature*, **569**, 265–269.

Feys, B.J., Wiermer, M., Bhat, R.A., Moisan, L.J., Medina-Escobar, N., Neu, C. et al. (2005) Arabidopsis SENESCENCE-ASSOCIATED GENE101 stabilizes and signals within an ENHANCED DISEASE SUSCEPTIBILITY1 complex in plant innate immunity. *Plant Cell*, **17**, 2601–2613.

Garner, C.M., Spears, B.J., Su, J., Cseke, L.J., Smith, S.N., Rogan, C.J. et al. (2021) Opposing functions of the plant TOPLESS gene family during SNC1-mediated autoimmunity. *PLoS Genetics*, **17**, e1009026.

Geldner, N., Dénervaud-Tendon, V., Hyman, D.L., Mayer, U., Stierhof, Y.-D. & Chory, J. (2009) Rapid, combinatorial analysis of membrane compartments in intact plants with a multicolor marker set. *The Plant Journal*, **59**, 169–178.

Gillingham, A.K. & Munro, S. (2003) Long coiled-coil proteins and membrane traffic. *Biochimica et Biophysica Acta*, **1641**, 71–85.

Gimenez-Ibanez, S., Ntoukakis, V. & Rathjen, J.P. (2009) The LysM receptor kinase CERK1 mediates bacterial perception in Arabidopsis. *Plant Signaling & Behavior*, **4**, 539–541.

Glazebrook, J., Zook, M., Mert, F., Kagan, I., Rogers, E.E., Crute, I.R. et al. (1997) Phytoalexin-deficient mutants of Arabidopsis reveal that PAD4 encodes a regulatory factor and that four PAD genes contribute to downy mildew resistance. *Genetics*, **146**, 381–392.

Gómez-Gómez, L. & Boller, T. (2000) FLS2: an LRR receptor-like kinase involved in the perception of the bacterial elicitor flagellin in Arabidopsis. *Molecular Cell*, **5**, 1003–1011.

Goodstein, D.M., Shu, S., Howson, R., Neupane, R., Hayes, R.D., Fazo, J. et al. (2012) Phytozome: a comparative platform for green plant genomics. *Nucleic Acids Research*, **40**, D1178–D1186.

Gou, M., Shi, Z., Zhu, Y., Bao, Z., Wang, G. & Hua, J. (2012) The F-box protein CPR1/CPR30 negatively regulates R protein SNC1 accumulation. *The Plant Journal*, **69**, 411–420.

Grigoriev, I.V., Hayes, R.D., Calhoun, S., Kamel, B., Wang, A., Ahrendt, S. et al. (2021) PhycoCosm, a comparative algal genomics resource. *Nucleic Acids Research*, **49**, D1004–D1011.

Hartmann, M., Zeier, T., Bernsdorff, F., Reichel-Deland, V., Kim, D., Hohmann, M. et al. (2018) Flavin monooxygenase-generated N-Hydroxypipecolic acid is a critical element of plant systemic immunity. *Cell*, **173**, 456–469.e16.

Horsefield, S., Burdett, H., Zhang, X., Manik, M.K., Shi, Y., Chen, J. et al. (2019) NAD+ cleavage activity by animal and plant TIR domains in cell death pathways. *Science*, **365**, 793–799.

Huang, J., Zhu, C. & Li, X. (2018) SCFSNIPER4 controls the turnover of two redundant TRAF proteins in plant immunity. *The Plant Journal*, **95**, 504–515.

Huang, S., Chen, X., Zhong, X., Li, M., Ao, K., Huang, J. et al. (2016) Plant TRAF proteins regulate NLR immune receptor turnover. *Cell Host & Microbe*, **19**, 204–215.

Huang, S., Jia, A., Song, W., Hessler, G., Meng, Y., Sun, Y. et al. (2022) Identification and receptor mechanism of TIR-catalyzed small molecules in plant immunity. *Science*, **377**, eabq3297. Available from: https://doi.org/10.1101/2022.04.01.486681

Huang, X., Li, J., Bao, F., Zhang, X. & Yang, S. (2010) A gain-of-function mutation in the Arabidopsis disease resistance gene RPP4 confers sensitivity to low temperature. *Plant Physiology*, **154**, 796–809.

Hulbert, S.H., Webb, C.A., Smith, S.M. & Sun, Q. (2001) Resistance gene complexes: evolution and utilization. *Annual Review of Phytopathology*, **39**, 285–312.

Jacob, F., Vernaldi, S. & Maekawa, T. (2013) Evolution and conservation of plant NLR functions. *Frontiers in Immunology*, **4**, 297.

Jacob, P., Kim, N.H., Wu, F., El-Kasmi, F., Chi, Y., Walton, W.G. et al. (2021) Plant "helper" immune receptors are Ca2+−permeable nonselective cation channels. *Science*, **373**, 420–425.

Jia, A., Huang, S., Song, W., Wang, J., Meng, Y., Sun, Y. et al. (2022) TIR-catalyzed ADP-ribosylation reactions produce signaling molecules for plant immunity. *Science*, **377**, eabq8180. Available from: https://doi.org/10.1101/2022.05.02.490369

Johnson, K.C.M., Dong, O.X., Huang, Y. & Li, X. (2012) A rolling stone gathers no moss, but resistant plants must gather their moses. *Cold Spring Harbor Symposia on Quantitative Biology*, **77**, 259–268.

Jones, J.D.G., Vance, R.E. & Dangl, J.L. (2016) Intracellular innate immune surveillance devices in plants and animals. *Science*, **354**, aaf6395.

Jones, P., Binns, D., Chang, H.-Y., Fraser, M., Li, W., McAnulla, C. et al. (2014) InterProScan 5: genome-scale protein function classification. *Bioinformatics*, **30**, 1236–1240.

Juranič, M., Srilunchang, K., Krohn, N.G., Leljak-Levanic, D., Sprunck, S. & Dresselhaus, T. (2012) Germline-specific MATH-BTB substrate adaptor MAB1 regulates spindle length and nuclei identity in maize. *Plant Cell*, **24**, 4974–4991.

Kalyaanamoorthy, S., Minh, B.Q., Wong, T.K.F., von Haeseler, A. & Jermiin, L.S. (2017) ModelFinder: fast model selection for accurate phylogenetic estimates. *Nature Methods*, **14**, 587–589.

Katoh, K. & Standley, D.M. (2013) MAFFT multiple sequence alignment software version 7: improvements in performance and usability. *Molecular Biology and Evolution*, **30**, 772–780.

Kim, S.H., Gao, F., Bhattacharjee, S., Adiasor, J.A., Nam, J.C. & Gassmann, W. (2010) The Arabidopsis resistance-like gene SNC1 is activated by mutations in SRFR1 and contributes to resistance to the bacterial effector AvrRps4. *PLoS Pathogens*, **6**, e1001172.

Kushwaha, H.R., Joshi, R., Pareek, A. & Singla-Pareek, S.L. (2016) MATH-domain family shows response toward abiotic stress in Arabidopsis and Rice. *Frontiers in Plant Science*, **7**, 923.

Kwon, S.I., Kim, S.H., Bhattacharjee, S., Noh, J.-J. & Gassmann, W. (2009) SRFR1, a suppressor of effector-triggered immunity, encodes a conserved tetratricopeptide repeat protein with similarity to transcriptional repressors. *The Plant Journal*, **57**, 109–119.

Lapin, D., Bhandari, D.D. & Parker, J.E. (2020) Origins and immunity networking functions of EDS1 family proteins. *Annual Review of Phytopathology*, **58**, 253–276.

Lapin, D., Johanndrees, O., Wu, Z., Li, X. & Parker, J.E. (2022) Molecular innovations in plant TIR-based immunity signaling. *Plant Cell*, **34**, 1479–1496.

Lapin, D., Kovacova, V., Sun, X., Dongus, J.A., Bhandari, D., von Born, P. et al. (2019) A coevolved EDS1-SAG101-NRG1 module mediates cell death signaling by TIR-domain immune receptors. *Plant Cell*, **31**, 2430–2455.

Leliaert, F., Smith, D.R., Moreau, H., Herron, M.D., Verbruggen, H., Delwiche, C.F. et al. (2012) Phylogeny and molecular evolution of the green algae. *Critical Reviews in Plant Sciences*, **31**, 1–46.

Li, F.-W., Brouwer, P., Carretero-Paulet, L., Cheng, S., de Vries, J., Delaux, P.-M. et al. (2018) Fern genomes elucidate land plant evolution and cyanobacterial symbioses. *Nature Plants*, **4**, 460–472.

Li, X., Clarke, J.D., Zhang, Y. & Dong, X. (2001) Activation of an EDS1-mediated R-gene pathway in the snc1 mutant leads to constitutive, NPR1-independent pathogen resistance. *Molecular Plant-Microbe Interactions*, **14**, 1131–1139.

Li, X., Kapos, P. & Zhang, Y. (2015) NLRs in plants. *Current Opinion in Immunology*, **32**, 114–121.

Li, Y., Li, S., Bi, D., Cheng, Y.T., Li, X. & Zhang, Y. (2010) SRFR1 negatively regulates plant NB-LRR resistance protein accumulation to prevent autoimmunity. *PLoS Pathogens*, **6**, e1001111.

Liu, H., Ding, Y., Zhou, Y., Jin, W., Xie, K. & Chen, L.-L. (2017) CRISPR-P 2.0: an improved CRISPR-Cas9 tool for genome editing in plants. *Molecular Plant*, **10**, 530–532.

Liu, J., Ding, P., Sun, T., Nitta, Y., Dong, O., Huang, X. et al. (2013) Heterotrimeric G proteins serve as a converging point in plant defense signaling activated by multiple receptor-like kinases. *Plant Physiology*, **161**, 2146–2158.

Lu, Y., Wu, T., Gutman, O., Lu, H., Zhou, Q., Henis, Y.I. et al. (2020) Phase separation of TAZ compartmentalizes the transcription machinery to promote gene expression. *Nature Cell Biology*, **22**, 453–464.

Ma, S., Lapin, D., Liu, L., Sun, Y., Song, W., Zhang, X. et al. (2020) Direct pathogen-induced assembly of an NLR immune receptor complex to form a holoenzyme. *Science*, **370**, eabe3069.

Madeira, F., Park, Y.M., Lee, J., Buso, N., Gur, T., Madhusoodanan, N. et al. (2019) The EMBL-EBI search and sequence analysis tools APIs in 2019. *Nucleic Acids Research*, **47**, W636–W641.

Madison, W. & Madison, D. (2019) Mesquite: a modular system for evolutionary analysis. Advance Access published 2019.

Manik, M.K., Shi, Y., Li, S., Zaydman, M.A., Damaraju, N., Eastman, S. et al. (2022) Cyclic ADP ribose isomers: production, chemical structures, and immune signaling. *Science*, **377**, eadc8969. Available from: https://doi.org/10.1101/2022.05.07.491051

Mao, Y., Zhang, H., Xu, N., Zhang, B., Gou, F. & Zhu, J.-K. (2013) Application of the CRISPR-Cas system for efficient genome engineering in plants. *Molecular Plant*, **6**, 2008–2011.

Martin, R., Qi, T., Zhang, H., Liu, F., King, M., Toth, C. et al. (2020) Structure of the activated ROQ1 resistosome directly recognizing the pathogen effector XopQ. *Science*, **370**, eabd9993.

Maruri-López, I., Figueroa, N.E., Hernández-Sánchez, I.E. & Chodasiewicz, M. (2021) Plant stress granules: trends and beyond. *Frontiers in Plant Science*, **12**, 722643.

Meyers, B.C., Kozik, A., Griego, A., Kuang, H. & Michelmore, R.W. (2003) Genome-wide analysis of NBS-LRR-encoding genes in Arabidopsis. *Plant Cell*, **15**, 809–834.

Miao, M., Niu, X., Kud, J., Du, X., Avila, J., Devarenne, T.P. et al. (2016) The ubiquitin ligase SEVEN IN ABSENTIA (SINA) ubiquitinates a defense-related NAC transcription factor and is involved in defense signaling. *The New Phytologist*, **211**, 138–148.

Michelmore, R.W. & Meyers, B.C. (1998) Clusters of resistance genes in plants evolve by divergent selection and a birth-and-death process. *Genome Research*, **8**, 1113–1130.

Minh, B.Q., Schmidt, H.A., Chernomor, O., Schrempf, D., Woodhams, M.D., von Haeseler, A. et al. (2020) IQ-TREE 2: new models and efficient methods for phylogenetic inference in the genomic era. *Molecular Biology and Evolution*, **37**, 1530–1534.

Minkenberg, B., Zhang, J., Xie, K. & Yang, Y. (2019) CRISPR-PLANT v2: an online resource for highly specific guide RNA spacers based on improved off-target analysis. *Plant Biotechnology Journal*, **17**, 5–8.

Mitchell, A.L., Attwood, T.K., Babbitt, P.C., Blum, M., Bork, P., Bridge, A. et al. (2019) InterPro in 2019: improving coverage, classification and access to protein sequence annotations. *Nucleic Acids Research*, **47**, D351–D360.

Monaghan, J., Xu, F., Gao, M., Zhao, Q., Palma, K., Long, C. et al. (2009) Two Prp19-like U-box proteins in the MOS4-associated complex play redundant roles in plant innate immunity. *PLoS Pathogens*, **5**, e1000526.

Mudgil, Y., Shiu, S.-H., Stone, S.L., Salt, J.N. & Goring, D.R. (2004) A large complement of the predicted Arabidopsis ARM repeat proteins are members of the U-box E3 ubiquitin ligase family. *Plant Physiology*, **134**, 59–66.

Necci, M., Piovesan, D., Clementel, D., Dosztányi, Z. & Tosatto, S.C.E. (2020) MobiDB-lite 3.0: fast consensus annotation of intrinsic disorder flavours in proteins. *Bioinformatics*, **36**, 5533–5534. Available from: https://doi.org/10.1093/bioinformatics/btaa1045

Nelson, B.K., Cai, X. & Nebenführ, A. (2007) A multicolored set of in vivo organelle markers for co-localization studies in Arabidopsis and other plants. *The Plant Journal*, **51**, 1126–1136.

Niu, D., Lin, X.-L., Kong, X., Qu, G.-P., Cai, B., Lee, J. et al. (2019) SIZ1-mediated SUMOylation of TPR1 suppresses plant immunity in Arabidopsis. *Molecular Plant*, **12**, 215–228.

Oates, M.E., Romero, P., Ishida, T., Ghalwash, M., Mizianty, M.J., Xue, B. et al. (2013) D^2P^2: database of disordered protein predictions. *Nucleic Acids Research*, **41**, D508–D516.

Oelmüller, R., Peškan-Berghöfer, T., Shahollari, B., Trebicka, A., Sherameti, I. & Varma, A. (2005) MATH domain proteins represent a novel protein family in Arabidopsis thaliana, and at least one member is modified in roots during the course of a plant–microbe interaction. *Physiologia Plantarum*, **124**, 152–166.

One Thousand Plant Transcriptomes Initiative. (2019) One thousand plant transcriptomes and the phylogenomics of green plants. *Nature*, **574**, 679–685.

Palma, K., Zhang, Y. & Li, X. (2005) An importin alpha homolog, MOS6, plays an important role in plant innate immunity. *Current Biology*, **15**, 1129–1135.

Palma, K., Zhao, Q., Cheng, Y.T., Bi, D., Monaghan, J., Cheng, W. et al. (2007) Regulation of plant innate immunity by three proteins in a complex conserved across the plant and animal kingdoms. *Genes & Development*, **21**, 1484–1493.

Park, H.H. (2018) Structure of TRAF family: current understanding of receptor recognition. *Frontiers in Immunology*, **9**, 1999.

Park, Y.C., Burkitt, V., Villa, A.R., Tong, L. & Wu, H. (1999) Structural basis for self-association and receptor recognition of human TRAF2. *Nature*, **398**, 533–538.

Pattengale, N.D., Alipour, M., Bininda-Emonds, O.R.P., Moret, B.M.E. & Stamatakis, A. (2009) How many bootstrap replicates are necessary? In: Batzoglou, S. (Ed.) *Research in computational molecular biology*. Berlin, Heidelberg: Springer Berlin Heidelberg, pp. 184–200.

Qi, H., Li, J., Xia, F.-N., Chen, J.-Y., Lei, X., Han, M.-Q. et al. (2020) Arabidopsis SINAT proteins control autophagy by mediating ubiquitylation and degradation of ATG13. *Plant Cell*, **32**, 263–284.

Qi, H., Xia, F.-N., Xiao, S. & Li, J. (2022) TRAF proteins as key regulators of plant development and stress responses. *Journal of Integrative Plant Biology*, **64**, 431–448.

Qi, H., Xia, F.-N., Xie, L.-J., Yu, L.-J., Chen, Q.-F., Zhuang, X.-H. et al. (2017) TRAF family proteins regulate autophagy dynamics by modulating AUTOPHAGY PROTEIN6 stability in Arabidopsis. *Plant Cell*, **29**, 890–911.

R Core Team. (2019) *R: A Language and Environment for Statistical Computing*. Vienna, Austria: R Foundation for Statistical Computing.

Roberts, M., Tang, S., Stallmann, A., Dangl, J.L. & Bonardi, V. (2013) Genetic requirements for signaling from an autoactive plant NB-LRR intracellular innate immune receptor. *PLoS Genetics*, **9**, e1003465.

Rueden, C.T., Schindelin, J., Hiner, M.C., DeZonia, B.E., Walter, A.E., Arena, E.T. et al. (2017) ImageJ2: ImageJ for the next generation of scientific image data. *BMC Bioinformatics*, **18**, 529.

Saur, I.M.L., Panstruga, R. & Schulze-Lefert, P. (2021) NOD-like receptor-mediated plant immunity: from structure to cell death. *Nature Reviews. Immunology*, **21**, 305–318.

Stamatakis, A. (2014) RAxML version 8: a tool for phylogenetic analysis and post-analysis of large phylogenies. *Bioinformatics*, **30**, 1312–1313.

Sun, T., Zhang, Y., Li, Y., Zhang, Q., Ding, Y. & Zhang, Y. (2015) ChIP-seq reveals broad roles of SARD1 and CBP60g in regulating plant immunity. *Nature Communications*, **6**, 10159.

Sun, X., Lapin, D., Feehan, J.M., Stolze, S.C., Kramer, K., Dongus, J.A. et al. (2021) Pathogen effector recognition-dependent association of NRG1 with EDS1 and SAG101 in TNL receptor immunity. *Nature Communications*, **12**, 3335.

Sun, Y., Zhu, Y.-X., Balint-Kurti, P.J. & Wang, G.-F. (2020) Fine-tuning immunity: players and regulators for plant NLRs. *Trends in Plant Science*, **25**, 695–713.

The 1001 Genomes Consortium. (2016) 1,135 genomes reveal the global pattern of polymorphism in Arabidopsis thaliana. *Cell*, **166**, 481–491.

The Angiosperm Phylogeny Group, Chase, M.W., Christenhusz, M.J.M., Fay, M.F., Byng, J.W., Judd, W.S. et al. (2016) An update of the angiosperm phylogeny group classification for the orders and families of flowering plants: APG IV. *Botanical Journal of the Linnean Society*, **181**, 1–20.

Thomas, J.H. (2006) Analysis of homologous gene clusters in Caenorhabditis elegans reveals striking regional cluster domains. *Genetics*, **172**, 127–143.

Thomas, P.D., Ebert, D., Muruganujan, A., Mushayahama, T., Albou, L.-P. & Mi, H. (2022) PANTHER: making genome-scale phylogenetics accessible to all. *Protein Science*, **31**, 8–22.

Tian, H., Wu, Z., Chen, S., Ao, K., Huang, W., Yaghmaiean, H. et al. (2021) Activation of TIR signalling boosts pattern-triggered immunity. *Nature*, **598**, 500–503.

Truebestein, L. & Leonard, T.A. (2016) Coiled-coils: the long and short of it. *BioEssays*, **38**, 903–916.

Tsuda, K. & Somssich, I.E. (2015) Transcriptional networks in plant immunity. *The New Phytologist*, **206**, 932–947.

Ullah, H., Chen, J.-G., Temple, B., Boyes, D.C., Alonso, J.M., Davis, K.R. et al. (2003) The beta-subunit of the Arabidopsis G protein negatively regulates auxin-induced cell division and affects multiple developmental processes. *Plant Cell*, **15**, 393–409.

UniProt Consortium. (2019) UniProt: a worldwide hub of protein knowledge. *Nucleic Acids Research*, **47**, D506–D515.

Uversky, V.N. (2017) Intrinsically disordered proteins in overcrowded milieu: membrane-less organelles, phase separation, and intrinsic disorder. *Current Opinion in Structural Biology*, **44**, 18–30.

Van Bel, M., Diels, T., Vancaester, E., Kreft, L., Botzki, A., Van de Peer, Y. et al. (2018) PLAZA 4.0: an integrative resource for functional, evolutionary and comparative plant genomics. *Nucleic Acids Research*, **46**, D1190–D1196.

van der Biezen, E.A., Freddie, C.T., Kahn, K., Parker, J.E. & Jones, J.D.G. (2002) Arabidopsis RPP4 is a member of the RPP5 multigene family of TIR-NB-LRR genes and confers downy mildew resistance through multiple signalling components. *The Plant Journal*, **29**, 439–451.

van Wersch, R., Li, X. & Zhang, Y. (2016) Mighty dwarfs: Arabidopsis autoimmune mutants and their usages in genetic dissection of plant immunity. *Frontiers in Plant Science*, **7**, 1717.

Waese, J., Fan, J., Pasha, A., Yu, H., Fucile, G., Shi, R. et al. (2017) ePlant: visualizing and exploring multiple levels of data for hypothesis generation in plant biology. *Plant Cell*, **29**, 1806–1821.

Wagner, S., Stuttmann, J., Rietz, S., Guerois, R., Brunstein, E., Bautor, J. et al. (2013) Structural basis for signaling by exclusive EDS1 heteromeric complexes with SAG101 or PAD4 in plant innate immunity. *Cell Host & Microbe*, **14**, 619–630.

Wan, L., Essuman, K., Anderson, R.G., Sasaki, Y., Monteiro, F., Chung, E.-H. et al. (2019) TIR domains of plant immune receptors are NAD+-cleaving enzymes that promote cell death. *Science*, **365**, 799–803.

Wang, W., Fan, Y., Niu, X., Miao, M., Kud, J., Zhou, B. et al. (2018) Functional analysis of the seven in absentia ubiquitin ligase family in tomato. *Plant, Cell & Environment*, **41**, 689–703.

Wang, Y., Zhang, Y., Wang, Z., Zhang, X. & Yang, S. (2013) A missense mutation in CHS1, a TIR-NB protein, induces chilling sensitivity in Arabidopsis. *The Plant Journal*, **75**, 553–565.

Wang, Z.-P., Xing, H.-L., Dong, L., Zhang, H.-Y., Han, C.-Y., Wang, X.-C. et al. (2015) Egg cell-specific promoter-controlled CRISPR/Cas9 efficiently generates homozygous mutants for multiple target genes in Arabidopsis in a single generation. *Genome Biology*, **16**, 144.

Waterhouse, A.M., Procter, J.B., Martin, D.M.A., Clamp, M. & Barton, G.J. (2009) Jalview Version 2—a multiple sequence alignment editor and analysis workbench. *Bioinformatics*, **25**, 1189–1191.

Wickham, H., Averick, M., Bryan, J., Chang, W., McGowan, L., François, R. et al. (2019) Welcome to the Tidyverse. *Journal of Open Source Software*, **4**, 1686.

Williams, S.J., Sohn, K.H., Wan, L., Bernoux, M., Sarris, P.F., Segonzac, C. et al. (2014) Structural basis for assembly and function of a heterodimeric plant immune receptor. *Science*, **344**, 299–303.

Wirthmueller, L., Roth, C., Banfield, M.J. & Wiermer, M. (2013) Hop-on hop-off: importin-α-guided tours to the nucleus in innate immune signaling. *Frontiers in Plant Science*, **4**, 149.

Wu, Z., Li, M., Dong, O.X., Xia, S., Liang, W., Bao, Y. et al. (2019) Differential regulation of TNL-mediated immune signaling by redundant helper CNLs. *The New Phytologist*, **222**, 938–953.

Wu, Z., Tian, L., Liu, X., Huang, W., Zhang, Y. & Li, X. (2022) The N-terminally truncated helper NLR NRG1C antagonizes immunity mediated

by its full-length neighbors NRG1A and NRG1B. *Plant Cell*, **34**, 1621–1640.

Wu, Z., Tian, L., Liu, X., Zhang, Y. & Li, X. (2021) TIR signal promotes interactions between lipase-like proteins and ADR1-L1 receptor and ADR1-L1 oligomerization. *Plant Physiology*, **187**, 681–686.

Wu, Z., Tong, M., Tian, L., Zhu, C., Liu, X., Zhang, Y. et al. (2020) Plant E3 ligases SNIPER1 and SNIPER2 broadly regulate the homeostasis of sensor NLR immune receptors. *The EMBO Journal*, **39**, e104915.

Xie, P. (2013) TRAF molecules in cell signaling and in human diseases. *Journal of Molecular Signaling*, **8**, 7.

Xing, H.-L., Dong, L., Wang, Z.-P., Zhang, H.-Y., Han, C.-Y., Liu, B. et al. (2014) A CRISPR/Cas9 toolkit for multiplex genome editing in plants. *BMC Plant Biology*, **14**, 327.

Xu, F., Kapos, P., Cheng, Y.T., Li, M., Zhang, Y. & Li, X. (2014) NLR-associating transcription factor bHLH84 and its paralogs function redundantly in plant immunity. *PLoS Pathogens*, **10**, e1004312.

Xu, F., Xu, S., Wiermer, M., Zhang, Y. & Li, X. (2012) The cyclin L homolog MOS12 and the MOS4-associated complex are required for the proper splicing of plant resistance genes. *The Plant Journal*, **70**, 916–928.

Xu, F., Zhu, C., Cevik, V., Johnson, K., Liu, Y., Sohn, K. et al. (2015) Autoimmunity conferred by chs3-2D relies on CSA1, its adjacent TNL-encoding neighbour. *Scientific Reports*, **5**, 8792.

Xu, S., Zhang, Z., Jing, B., Gannon, P., Ding, J., Xu, F. et al. (2011) Transportin-SR is required for proper splicing of resistance genes and plant immunity. *PLoS Genetics*, **7**, e1002159.

Yoshimoto, K., Hanaoka, H., Sato, S., Kato, T., Tabata, S., Noda, T. et al. (2004) Processing of ATG8s, ubiquitin-like proteins, and their deconjugation by ATG4s are essential for plant autophagy. *Plant Cell*, **16**, 2967–2983.

Yu, D., Song, W., Tan, E.Y.J., Liu, L., Cao, Y., Jirschitzka, J. et al. (2022) TIR domains of plant immune receptors are 2′,3′-cAMP/cGMP synthetases mediating cell death. *Cell*, **185**, 2370–2386.e18. Available from: https://doi.org/10.1016/j.cell.2022.04.032

Yu, G. (2022) *Data Integration, Manipulation and Visualization of Phylogenetic Trees*. New York: Chapman and Hall/CRC.

Yuan, J. & He, S.Y. (1996) The pseudomonas syringae Hrp regulation and secretion system controls the production and secretion of multiple extracellular proteins. *Journal of Bacteriology*, **178**, 6399–6402.

Zapata, J.M., Martínez-García, V. & Lefebvre, S. (2007) Phylogeny of the TRAF/MATH domain. *Advances in Experimental Medicine and Biology*, **597**, 1–24.

Zhang, X., Bernoux, M., Bentham, A.R., Newman, T.E., Ve, T., Casey, L.W. et al. (2017) Multiple functional self-association interfaces in plant TIR domains. *Proceedings of the National Academy of Sciences of the United States of America*, **114**, E2046–E2052.

Zhang, Y., Cheng, Y.T., Bi, D., Palma, K. & Li, X. (2005) MOS2, a protein containing G-patch and KOW motifs, is essential for innate immunity in Arabidopsis thaliana. *Current Biology*, **15**, 1936–1942.

Zhang, Y., Goritschnig, S., Dong, X. & Li, X. (2003) A gain-of-function mutation in a plant disease resistance gene leads to constitutive activation of downstream signal transduction pathways in suppressor of npr1-1, constitutive 1. *Plant Cell*, **15**, 2636–2646.

Zhang, Y., Song, G., Lal, N.K., Nagalakshmi, U., Li, Y., Zheng, W. et al. (2019) TurboID-based proximity labeling reveals that UBR7 is a regulator of N NLR immune receptor-mediated immunity. *Nature Communications*, **10**, 3252.

Zhang, Y., Yang, Y., Fang, B., Gannon, P., Ding, P., Li, X. et al. (2010) Arabidopsis snc2-1D activates receptor-like protein-mediated immunity transduced through WRKY70. *Plant Cell*, **22**, 3153–3163.

Zhang, Z., Wu, Y., Gao, M., Zhang, J., Kong, Q., Liu, Y. et al. (2012) Disruption of PAMP-induced MAP kinase cascade by a pseudomonas syringae effector activates plant immunity mediated by the NB-LRR protein SUMM2. *Cell Host & Microbe*, **11**, 253–263.

Zhao, L., Huang, Y., Hu, Y., He, X., Shen, W., Liu, C. et al. (2013) Phylogenetic analysis of Brassica rapa MATH-domain proteins. *Current Genomics*, **14**, 214–223.

Zhu, Z., Xu, F., Zhang, Y., Cheng, Y.T., Wiermer, M., Li, X. et al. (2010) Arabidopsis resistance protein SNC1 activates immune responses through association with a transcriptional corepressor. *Proceedings of the National Academy of Sciences of the United States of America*, **107**, 13960–13965.